AD

NDL-TR-93

A SUPERCONDUCTING THIN-FILM NUCLEAR-PARTICLE DETECTOR

D. B. Sullivan

OCTOBER 1967

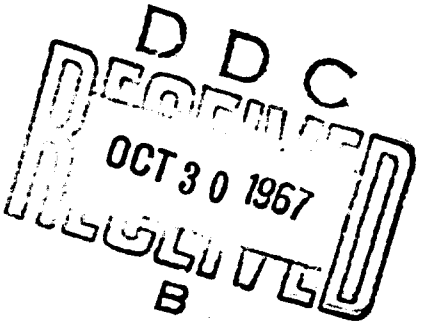

US ARMY
NUCLEAR DEFENSE LABORATORY
EDGEWOOD ARSENAL, MARYLAND

50

Disposition

Destroy this report when no longer needed. Do not return it to the originator.

Disclaimer

The findings in this report are not to be construed as an official Department of the Army position.

Trade Names Statement

Citation of trade names in this report does not constitute an official Department of the Army endorsement or approval of the use of such commercial items.

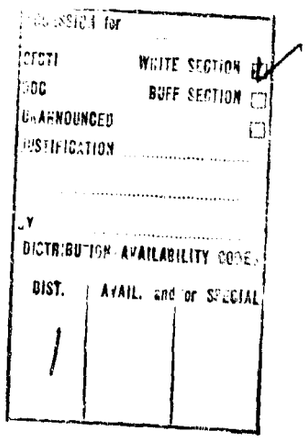

NDL-TR-93

A SUPERCONDUCTING THIN-FILM NUCLEAR-PARTICLE DETECTOR

D. B. Sullivan

October 1967

US ARMY
NUCLEAR DEFENSE LABORATORY
Edgewood Arsenal, Maryland

ABSTRACT

Recent advances in theory and development of a superconducting nuclear-particle detection technique are presented. A review of previous theory as well as recent theoretical work is included. Experimental results obtained at US Army Nuclear Defense Laboratory and through contract with Atomics International, a division of North American Aviation, are compared with the existing theory. The report is intended, not only to present results of recent work, but also to provide a summary of all developmental work. The problems encountered in the research are discussed and some suggestions are offered as possible paths to solutions.

ACKNOWLEDGEMENT

The author wishes to acknowledge the contribution of Dr. J.B. Greer, now with the Texas Company, who set up the cryogenic facility at this Laboratory, and to thank Mr. W.R. Van Antwerp of this Laboratory for his interest and critical review of this work. Mr. Van Antwerp should be credited with the motivation of both in-house and contractual activities in the development of this detector. The author would also like to thank Mr. Edward Kaufman of this Laboratory for assistance with the experiments and equipment and particularly for providing the detailed evaluation of one of the film fabrication techniques found in the Appendixes. Mr. Vincent Ribie of the Army Electronics Command has been most generous in providing the basis for initiation of work in photo-resist production of the detectors.

This work was funded by the NDL In-House Laboratory-Initiated Research and Development Project No. 1L013001A91A.

CONTENTS

A SUPERCONDUCTING
THIN-FILM NUCLEAR-PARTICLE DETECTOR

1. INTRODUCTION

1.1 Objective.

This document reports on the progress on development of a unique new nuclear-particle detector. The objective of this investigation is to develop an accurate theoretical model of the detector operation, and, with the aid of this model and experimental findings, to evaluate the potential applications of the detector. The detector is in an early stage of development and this report presents the results of recent theoretical and experimental work. A discussion of previous work on the detector is also included.

1.2 Background.

1.2.1 Historical Development of the Concept. The first direct observation of single particle events in superconducting materials is attributed to Andrews, et al.,[1] who held a thin strip of niobium nitride midway in the superconducting-to-normal transition region and were just able to detect pulses from incident alpha particles. Later, Sherman[2,3] introduced a theoretical treatment of the problem with a slightly different approach. In response to a request from the US Army Nuclear Defense Laboratory (USANDL), a contractual effort was undertaken by the Atomic International Division of North American Aviation to develop a detector based on these early ideas. The results of this work[4,5] were very promising and an in-house research program[6] on detector development was initiated. A brief summary of the theoretical contributions by the group at Atomics International is contained in Section 1.2.3. In addition, results of their experiments will be used at several junctures to ensure the broadest possible discussion of the overall development picture. Recent theoretical work at this Laboratory is presented in Section 2 and experimental results are presented and discussed in Section 3.

1.2.2 Merits of the Detector. A superconducting thin-film nuclear-particle detector is potentially as fast as any presently available particle detector, with theoretical risetimes in the subnanosecond to several nanosecond region. Equipment-limited risetimes of 3 to 4 ns have been observed. Improved detector output analysis will be needed to determine the limiting risetime of the detector. The detector can be operated in a position-sensitive mode, with positional resolution, along one dimension, of better than 100 μ. The work on the development of this aspect of the detector has not been extensive, but direct experimental evidence of feasibility has been obtained.

If future electronics for analysis of detector output is to be cryogenic, then the use of a superconducting detector would eliminate the need of coupling detector and electronics through a large temperature difference. In addition, the cryogenic operation of the detector may be an advantage where other components of the experimental scheme require cryogenic temperatures. If a figure of merit such as noise is associated with the resistivity of the detector, enormous advantages are offered by this superconducting device. The present detector geometry and mounting, while necessary for many testing purposes, does not offer a check of the noise figure. Presumably, a coaxial mounting of the detector will provide a significant noise reduction and facilitate the study of the noise inherent to the detector.

The section would not be complete without some discussion of the shortcomings of the detector, but it should be emphasized that these shortcomings, for the most part, are associated with the present form of the detector and that further investigation may clear the way for the removal of such limitations. The present detectors have active areas of about 10^{-3} cm^2, a far cry from those of semiconductor detectors. Volume of the detector is roughly 10^{-8} cm^3, another disappointingly low figure. In addition, attempts to obtain energy resolution from the detector have met with little success. According to the theory the pulse height from the detector should be roughly proportional to the square root of the stopping power, dE/dx. If, in the future, the dE/dx sensitivity is realized, then the relationship between the energy and dE/dx must be known in order to obtain the energy-pulse-height relation. Since the detector output is proportional to the square root of the stopping power, there is a limit to the mass and energy of the particles that can be detected. To date, only alpha particles in the 1 to 5 MeV region have been studied.

1.2.3 Theory of Pulse Formation. A simplified picture of the principle upon which the detector operates can be obtained by referring to Figures 1.1 and 1.2. An alpha particle passing through the narrow superconducting film causes a thin cylindrical core to revert to the normal state. As seen in Figure 1.1, the normal region diverts the supercurrent bias into the lateral regions, creating a momentary increase in the supercurrent density in those regions. The lateral regions will then revert to the normal state (see Figure 1.2) if the bias current is such that the critical current density, J_c, is exceeded in those lateral regions. The maximum radius of the normal core is labeled r_o. The progression to the state where a normal region extends across the film is accompanied by the appearance of a voltage across the region (by virtue of the bias current flowing in the detector). This normal region will then collapse if the Joule heating in it is smaller than the heat loss to the supporting substrate or, the region will expand (propagate) if the Joule heating is sufficiently large.

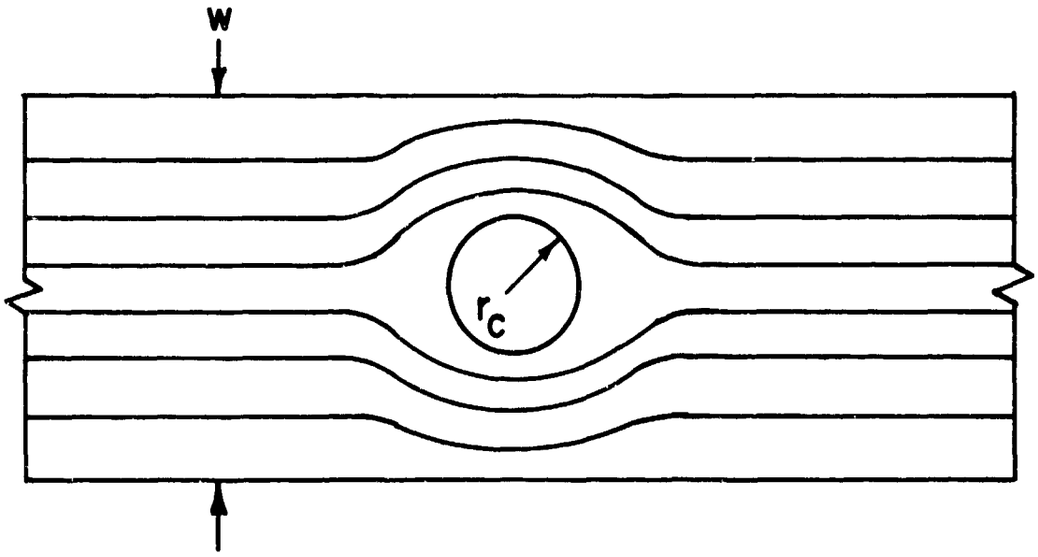

Figure 1.1 Normal region produced in a narrow current-carrying film by passage of an ionizing particle. Film width is w and the maximum normal-core radius is r_c.

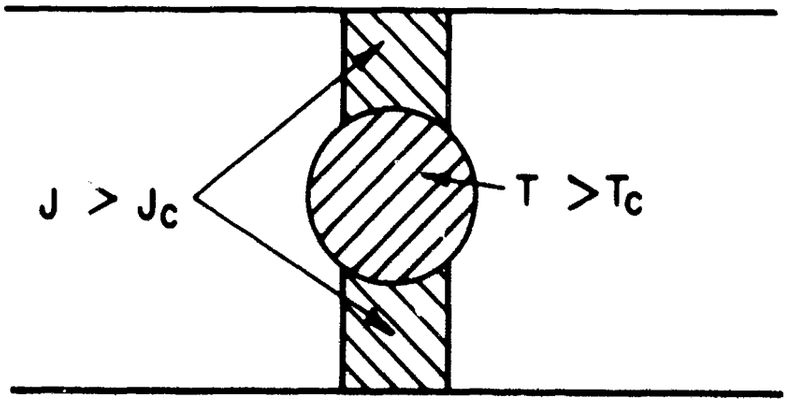

Figure 1.2 Current-induced transition of the regions lateral to the thermal core. The presence of the normal core causes the current density in the lateral regions to exceed the critical current density.

Figure 1.3 shows an example of the progression of the thermal profile in cylindrical geometry as taken from the theory to be summarized here. The passage of the ionizing particle through the film causes a very thin cylindrical core to revert to the normal state. This highly heated core then spreads and falls (thermal slump) as indicated in Figure 1.3. The intersection of the transition temperature, T_c, and the temperature profile defines the normal-core size. The normal-core radius increases to some maximum value, r_c, and then begins to decrease. It should be noted that the Joule heating which affects the extended normal region will not be included in the considerations of this section. Instead, the behavior of the thermal slump in an infinite-plane thin film (temperature profile with cylindrical symmetry) will be treated.

The thermodynamic treatment of the slump of the thermal spike follows Spiel, et al.,[4,5] at Atomics International. It is assumed that the electron mean free path is sufficiently small to warrant the application of classical thermodynamics to temperature profiles of such small dimension. This assumption has been the basis of considerable controversy, but it will suit the ends of this work to develop the theory on the basis of this assumption.

If it is assumed that the specific heat and thermal conductivity are of the same form (temperature dependence) in the superconducting and normal state, then the general diffusion equation which must be solved, can be written

$$k \nabla^2 T + \frac{dk}{dT} \left(\nabla T\right)^2 - C\rho \frac{\partial T}{\partial t} - \frac{\kappa}{d}\left(T - T_B \right) = 0 \quad , \qquad (1.1)$$

where k and C are respectively the thermal conductivity and the specific heat, ρ is the film density, d is the film thickness, κ is thermal conductance of the film-substrate boundary, T is the temperature of the film and T_B is the ambient (bath) temperature. The first two terms account for the rate at which heat enters and leaves a small volume element of the film; the third term represents the heat energy which goes into raising the temperature of the same volume element, and the last term gives a measure of the heat lost to the supporting substrate. In general, the specific heat and thermal conductivity have different dependences upon temperature in the superconducting and normal regions, and the solutions of two separate differential equations, one in each section, must be matched at the boundary to obtain the temperature profile as a function of time. The application of the results of the calculations and the expected differences between this and the simpler approach are such as to make this laborious calculation unwarranted.

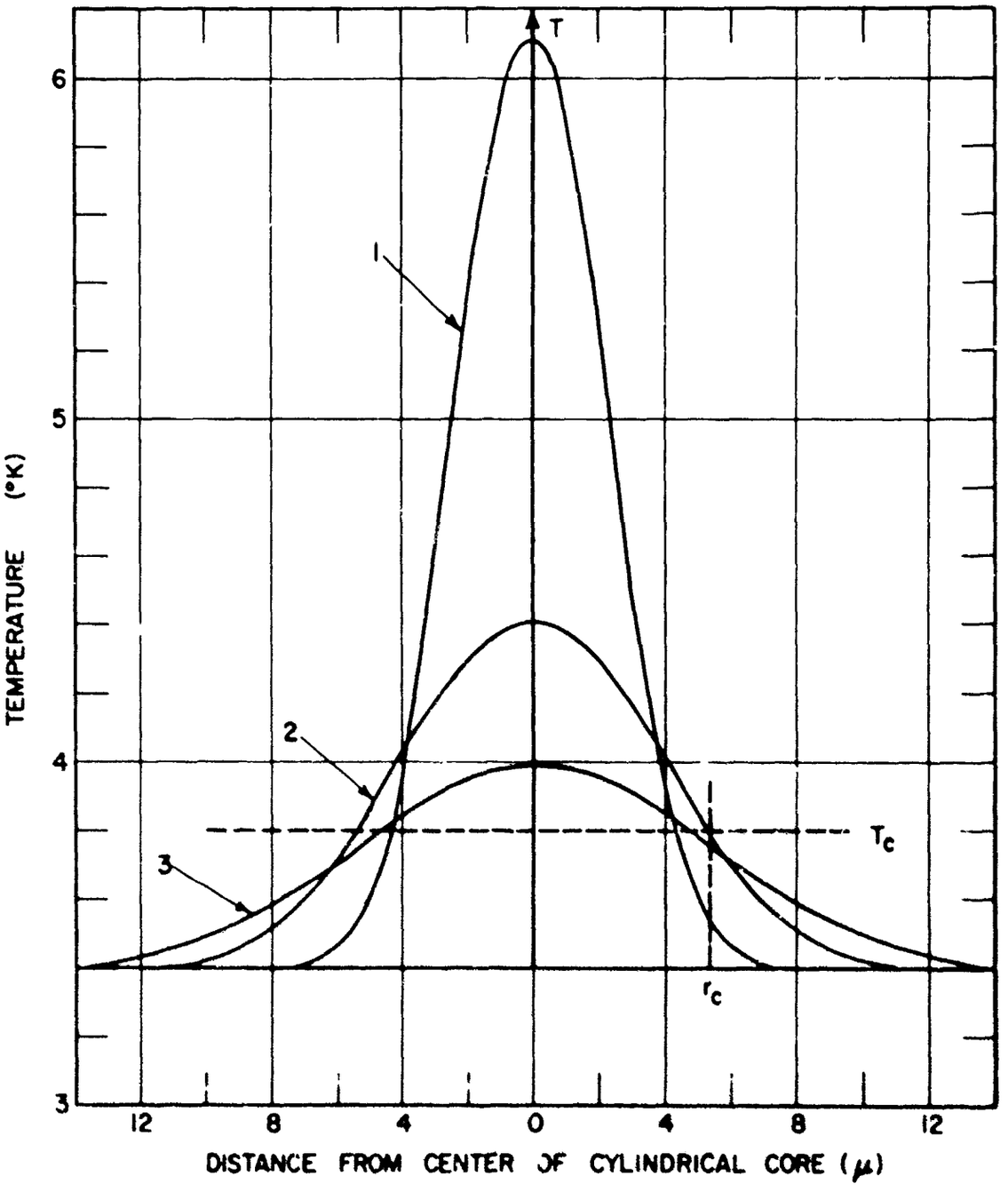

Figure 1.3 Slump of a thermal spike. The progression in time is in the same order as the curve numbering. The intersection of the profile with the transition temperature, T_c, defines the normal region which has a maximum radius, r_c.

To proceed with the solution of Equation 1.1 several additional simplifying assumptions were made. It was assumed that the last term in the equation, which accounts for the loss to the substrate, is negligible. The importance of this assumption will be discussed in detail in Section 3.3. Two different assumptions about the form of the thermal conductivity and specific heat were then tested. In one, the lattice and electronic components of both quantities were included and a computer solution of the equation was obtained. The second assumption used was that the energy imparted to the electrons in the film by the ionizing particle remains with the electrons for a sufficiently long period to warrant neglecting the lattice components of both specific heat and thermal conductivity. It is this latter approach which more closely fits the data and which will be presented here.

In this case the thermal conductivity and specific heat in the normal state take on the simple forms

$$k = L\sigma T \text{ and } C = \gamma T, \tag{1.2}$$

where L is the Lorenz number, σ is the electrical conductivity of the normal material (at low temperature), and γ is the Sommerfeld constant. With these values for k and C, Equation 1.1 takes on the particularly simple form

$$\frac{\partial}{\partial t} T^2 = \frac{L\sigma}{\gamma\rho} \nabla^2 T^2 \quad . \tag{1.3}$$

As boundary conditions, the temperature at distances infinite from the core which must be the bath temperature, T_B, and the peak temperature, T_o, of the initial core of radius b which must be obtained from the stopping power from the relation

$$- Q = \frac{dE}{dx} = \pi\rho b^2 \int_{T_o}^{T_B} \gamma T dT \quad . \tag{1.4}$$

The final solution is independent of b and T_o if observation is restricted to times greater than 10^{-12} seconds after the energy is deposited. The temperature profile in this case is

$$T^2 = T_B^2 + \frac{Q}{2\pi\rho\gamma Dt} e^{-r^2/4Dt} \quad , \tag{1.5}$$

where

$$D = \frac{L\sigma}{\gamma\rho} \quad . \tag{1.6}$$

The thermal profiles of Figure 1.3 were calculated from this formula.

The maximum normal radius, r_c, which is referred to as the critical radius, is obtained directly from this slumping profile and can be written

$$r_c^2 = \frac{2Q}{\pi e \rho \gamma (T_c^2 - T_B^2)} \quad . \tag{1.7}$$

If r_c is significantly bigger than half the film width (and if propagation does not occur) then a good estimate of r_c can be obtained from a measurement of the output-pulse amplitude and the bias current (since the normal-state resistance of the film is known). For values of r_c that are smaller than half the film width, a rough measurement of r_c can be obtained in the following manner. At a fixed temperature, the minimum current at which a pulse is formed, I_n, should be related to the available film width, $w - 2r_c$, in the same manner that the critical current, I_c, is related to the total film width. The critical current is, ideally, directly proportional to the film width and hence the following ratio can be formed:

$$\frac{I_n}{I_c} = \frac{w - 2r_c}{w} \quad \text{or} \quad r_c = \frac{w}{2}\left(1 - \frac{I_n}{I_c}\right) \quad . \tag{1.8}$$

Thus a measurement of the two threshold currents as a function of temperature will yield the temperature dependence of r_c for the case where r_c is small compared to half the film width.

These rough measurements of the critical radii can then be compared with the predicted values from Equation 1.7. It should be noted that the time interval between particle incidence and attainment of r_c is given by

$$t_c = \frac{1}{4D} r_c^2 \quad . \tag{1.9}$$

It is assumed that superconducting-to-normal transition times are sufficiently rapid to warrant the use of Equation 1.9 in making estimates of expected rise times.

1.3 Calculation of Detector Threshold Curves.

1.3.1 Threshold for Propagating Transition. Once a normal region is formed that extends across the film width, the differential equation governing the behavior of this normal region must be modified to include the Joule heating which occurs in it. The growth or decay of this normal region is dependent on the balance between the heat generated in the film and the loss to the substrate. As the Joule heating is current dependent, this growth or decay will depend on current level in the detector. The minimum current or threshold for propagation, I_p, is of considerable interest and will be considered in this section.

For simplicity the problem will be considered in one dimension; that is, the boundary between the superconducting and normal regions is assumed to be a plane moving along the one-dimensional film length, x. The losses to the substrate are perpendicular to the propagational direction, but this dimension does not enter the differential equation as a variable. The pertinent diffusion equation takes the form[7,8]

$$\kappa \frac{\partial^2 T}{\partial x^2} + \frac{dk}{dT}\left(\frac{\partial T}{\partial x}\right)^2 - C\rho\frac{\partial T}{\partial t} - \frac{\kappa}{d}\left(T-T_B\right) + \frac{j^2}{\sigma} = 0 \quad , \tag{1.10}$$

where j is the current density and σ is the normal-state electrical conductivity of the film. The temperature dependence of the electrical conductivity over the temperature range of interest is so slight that it is neglected.

The criterion for propagation is arrived at in the following manner. It is assumed that the film is infinitely long and that all film from x = 0 to x = ∞ is superconducting and that from x = 0 to x = - ∞ is normal. For the propagational velocity to be zero, the temperature profile must be static; that is, $\partial T/\partial t = 0$. As x goes to - ∞ the temperature must approach a constant value, $T_{-\infty}$, which is greater than T_c. Thus the derivatives of T with respect to position are zero at - ∞, and Equation 1.10 becomes

$$T_{-\infty} - T_B = \frac{d}{\kappa\sigma} j_p^2 \quad , \tag{1.11}$$

where j_p is the current density required for propagation.

Broom and Rhoderick[8] have shown that the peak temperature in the normal material, $T_{-\infty}$, for the case of constant thermal conductivity and specific heat, can be written in the form

$$T_{-\infty} = T_c + \frac{1}{2}\frac{d}{\kappa\sigma} j_p^2 \quad . \tag{1.12}$$

Combining Equations 1.11 and 1.12 yields

$$T_c - T_B = \frac{1}{2}\frac{d}{\kappa\sigma} j_p^2 \quad . \tag{1.13}$$

For the purposes of presenting a qualitative description of the threshold curves, the tedious task of determining $T_{-\infty}$ for the case of temperature-dependent thermal conductivity and specific heat is not warranted.

The transition temperature, T_c, is a function of the bias current and can be represented in this case by

$$T_c = T_o \left(1 - \frac{I}{I_o}\right)^{1/2} \quad , \tag{1.14}$$

where T_o is the transition temperature at zero current and I_o is the critical current at zero temperature. Note that I/I_o is equal to j/j_c, where j_o is the critical current density at zero temperature. Equations 1.13 and 1.14 are combined to eliminate T_c with the result,

$$T_B = T_o \left(1 - i_p\right)^{1/2} - \frac{j_o^2 d}{2\kappa\sigma} i_p^2 \quad , \tag{1.15}$$

where $i_p = I_p/I_o = j_p/j_o$. This relation can be solved to give the dependence of the threshold for propagation, i_p, on the bath temperature.

This represents the upper bound for any pulse propagation, for if only a short length of the film is normal, the current required to cause propagation is slightly less than that required for the normal region of infinite extent. If the current through the short region is the same as the threshold for the infinite case, the average temperature and hence the heat lost to the substrate would be smaller, causing the smaller region to expand towards the treated case. For the films studied, it has been shown[9] that the temperature profile is such as to require normal regions of only 10^{-2} cm in length to fit the infinite-length assumption. In other words the temperature varies from the bath temperature to the peak temperature over distances smaller than 10^{-2} cm. Hence, Equation 1.15 can be used to represent the propagational threshold for the case of small-finite normal regions.

It is interesting to note that i_p depends only on the film thickness, d, and not on the width. The effect of altering the width is to alter the power input to the film (at the propagational threshold) and to simultaneously alter the heat loss to the substrate. The two quantities vary in such a fashion that i_p does not depend on the width. Of course i_p is the reduced current, I_p/I_o, and I_p is a function of width in as much as I_o is. Similar reasoning leads one to accept the dependence of i_p on the film thickness as a quite reasonable result.

1.3.2 Threshold for Pulse Formation. The theoretical development of Section 1.2.3 can be utilized to calculate the threshold current, I_n, for the formation of a resistive region across the film width. In that Section it was shown how the value of the critical radius, r_c, could be obtained from experiment for comparison with theory. A reasonable prediction of this

threshold current can be obtained by a straightforward combination of Equations 1.7, 1.8, and 1.14. An assumption inherent to this approach is that the superconducting material outside the normal region is all at the bath temperature when, in fact, the temperature decreases from T_c at the boundary to the bath temperature (in the superconducting region). The effect of this increased temperature in the superconducting region is to reduce the critical current density in the region. This section will present an approach to accounting for this effect.

The idea is to assume that the critical-current density is the same function of temperature that the critical current is and further to assume that the current just prior to the transition (current-induced) is distributed in such a way that every element is at the critical point (i.e. $j = j_c$ at every point along the temperature profile in the superconducting region). Rearranging Equation 1.14 one obtains the following form for the critical current density:

$$j_c = j_o \left[1 - \left(\frac{T}{T_o}\right)^2\right] \quad . \tag{1.16}$$

For the sake of visualizing the problem, the normal core at maximum size is taken to be time independent (that is, the temperature distribution is not changing in time). Then, if we envision increasing the current until a transition of the lateral areas (see Figure 1.2) occurs, the threshold for the formation of a pulse is defined. Substituting the temperature profile into Equation 1.16 one obtains

$$\frac{j_c}{j_o} = \left[1 - \left(\frac{T_s}{T_o}\right)^2 - \frac{Q}{2\pi D\rho\gamma T_c^2} e^{-r^2/4Dt}\right] \quad . \tag{1.17}$$

Normally, the time at which the integrated current density is a minimum would seem to correspond to the time, t_o, at which the critical radius is formed. However, there is a possibility that this is not true and it is better to leave this time variable and minimize the threshold current with respect to it.

The threshold current, I_n, for the formation of a resistive region across the film width is then given by

$$I_n = \int_A j_c \, dA = d \int_r j_c \, dr \quad , \tag{1.18}$$

where the first integral is over the cross-sectional area of the superconducting region and the second is across the portion of the film width which remains superconducting. The critical current at zero temperature (no incident ionizing particles) is $I_o = j_o wd$. Thus the integral of Equation 1.18 can be rewritten as

$$\frac{I_n}{I_o} = i_n = \frac{1}{w}\int_r \frac{j_c}{j_o}\, dr \quad . \tag{1.19}$$

It is assumed that the minimum threshold for particles that hit the midway point between the film edges is representative and hence if the distance from the center to the boundary between the superconducting and normal regions is labeled r_b, then the threshold is given by

$$i_n = \frac{2}{w}\int_{r_b}^{w/2} \frac{j_c}{j_o}\, dr \quad . \tag{1.20}$$

This integral is then minimized with respect to time to give the threshold current (j_c/j_o is given by Equation 1.17). The values of t and r_b for this minimum correspond closely with those obtained from the thermal spike theory. It is important to note that i_n depends only on w (in as much as j_o can be considered to be independent of w). The results of this section as well as those of the previous one will be summarized graphically in the next section.

The effect of including the current limitation due to the heating in the superconducting region is more pronounced for the narrow films. The wider-film characteristics are hardly affected by this refinement. The inclusion of this refinement for the narrower films seems to agree better with experiment than the simpler approach.

1.3.3 Composite Picture of Detector Thresholds. Before presenting the composite description of the threshold curves, it is worth noting that there is an additional threshold which is actually more of an apparent threshold than a real one. This is the threshold above which the pulses can be observed through the noise. Since the measurements reflect the existence of this threshold, it is worth including.

It is assumed that the peak voltage of the smallest observable pulse, V_s, can be written as

$$V_s = I_s R \approx I_s (2r_c)\frac{1}{wd\sigma} \quad , \tag{1.21}$$

where I_s is the threshold current for pulse observation. Letting $i_s = I_s/I_o$ and using the earlier expression for r_c, one finds the relation between i_s and T_s to be

$$T_B = \sqrt{T_o^2 \left(1 - i_a\right) - \left(\frac{8Qj_o}{V_a \pi e \rho \gamma \sigma}\right)^2 i_a^2} \quad . \qquad (1.22)$$

If j_o and σ are assumed (to first approximation) to be independent of width and thickness, then this threshold is also independent of these quantities.

The set of threshold curves will now be plotted with width and thickness as variable parameters. The values of the constants that appear in the equations will be appropriate to those for tin with 5 MeV alpha particles as the incident radiation. These constants are listed in Table 1.1, below. The resistivity and the critical current density are representative of those measured for the array of available samples. It must be pointed out that the quantities in Table 1.1 are not all completely independent of the experimental arrangement (width and length of film in particular). The curves in the next few figures are intended to give a first approximation of the general behavior of the detector.

TABLE 1.1 VALUES OF CONSTANTS APPEARING IN EQUATIONS 1.1 THROUGH 1.22.

Constant	Value
Material	Tin
Transition Temperature	$T_c = 3.8^\circ$ K
Density	$\rho = 7.3$ g cm^{-3}
Electrical Conductivity	$\sigma = 1 \times 10^6$ mhos cm^{-1}
Critical Current Density at 0° K	$j_o = 4 \times 10^6$ A cm^{-2}
Stopping Power	$Q = 4 \times 10^{-10}$ J cm^{-2}
Sommerfelds Constant	$\gamma = 1.55 \times 10^{-5}$ J g^{-1} deg^{-2}
Lorenz Number	$L = 2.45 \times 10^{-8}$ V^2 deg^{-2}

Figure 1.4 shows the threshold curves for a film of 1000 Å thickness and a width of 10 μ. At this point there is one parameter in the equations that must be adjusted. This is the value of the boundary thermal conductance, κ, for which there is no reliable estimate in the literature because the boundary conductance is highly dependent upon the physical preparation of the interface surfaces. For these calculations the value of κ is set for the case depicted in Figure 1.4. The value of κ is adjusted so that the threshold for propagation passes through the point indicated on the graph. This point is chosen to give a fair agreement with experiment for

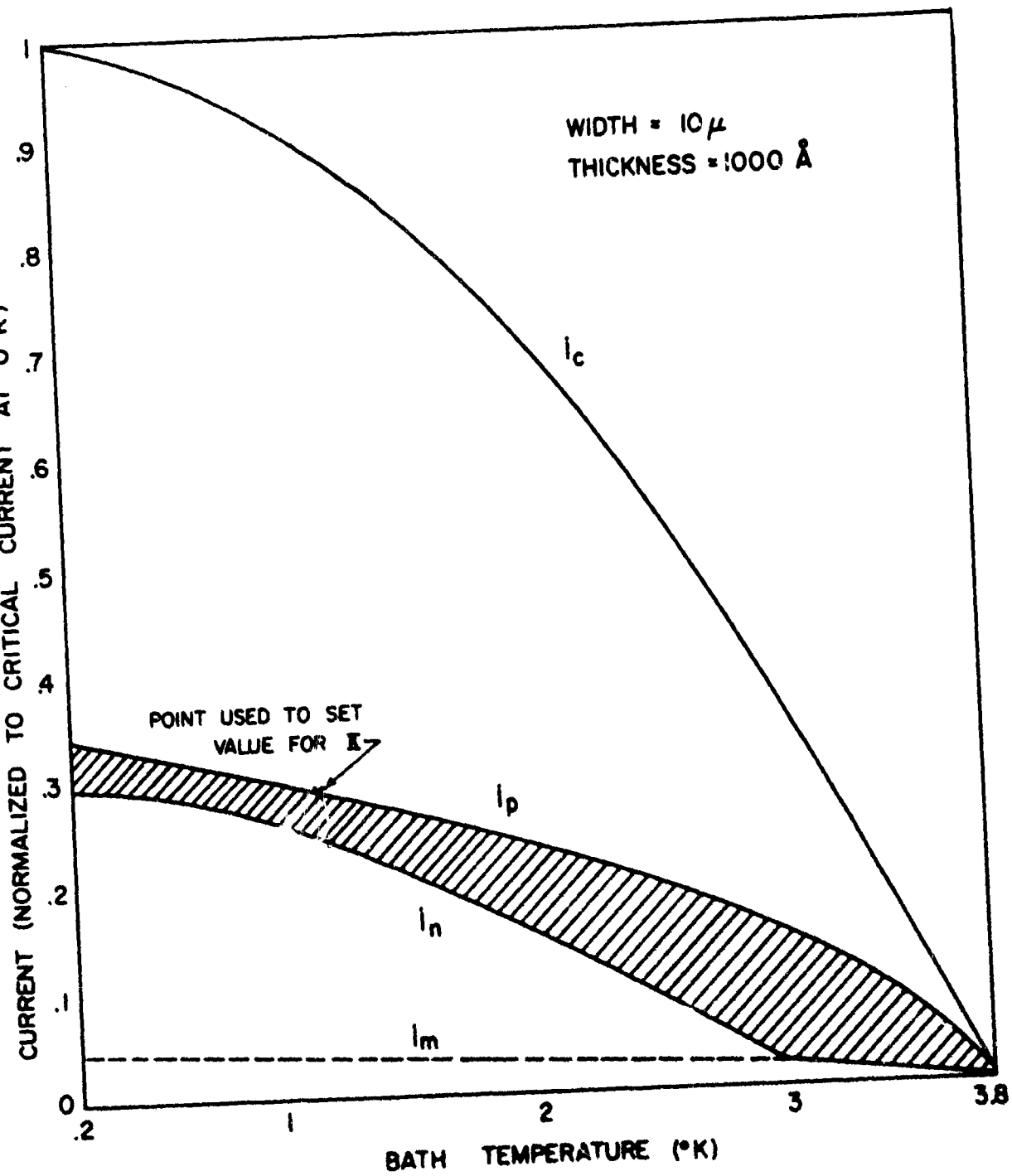

Figure 1.4 First approximation of the threshold curves for a tin film with incident 5 MeV alpha particles; i_c is the critical current; i_p is the threshold for propagating transitions; i_n is the threshold for formation of a normal region across the film width; and i_m represents the equipment limitation on pulse observation.

this particular film size. The value of κ obtained in this fashion is 3 W cm^{-2} deg^{-1} which falls well in the region of other values from the literature. The thermal conductance is then considered fixed at this value for all successive considerations.

As seen in Figure 1.4, the effect of the existence of the threshold for pulse observation is to cut off the lower portion of the non-propagating pulse region. For all figures which follow, the extension of this lower threshold will be excluded since it has no extensive significance. Below i_n there are no resistive pulses observed. Between i_n and i_p, pulses that are self-recovering (nonpropagating) are observed. And above i_p the pulse propagates down the film causing a complete transition to the normal state. The curve labeled i_c is the critical current of the film without incident radiation. Figures 1.5 and 1.6 indicate the expected variation of the detector's behavior with width. Notice that the only threshold that changes with width is i_n. The dashed portions of i_p are not measured directly in these experiments, because, while propagation can occur, above this curve there is nothing to initiate it. Thus, in the case where the curves cross, the propagating transition is not initiated until the current level is brought up to the threshold for resistive-region formation, i_n.

In Figures 1.7, 1.8 and 1.9 the width is held constant at 10 μ and the thickness is varied. In this case the only threshold curve which changes is i_p. For thicker films the variation of the threshold curves with thickness is not extremely pronounced because only a short portion of i_p can be observed. For very narrow films a sizeable effect should be seen as the film thickness is lowered below 1000 Å. There is a considerable bit of information contained in the graphs and calculations of this section and a further discussion of these considerations and their relation to experiment will be found in subsequent sections.

2. PROCEDURES

2.1 Film Preparation.

The most critical phase of detector fabrication is that of controlling the width of the film. To this end, three approaches have been considered in this work. The first approach (which has produced most of the usable detectors) requires two closely spaced razor blades to define the film. The razor-blade mask is in contact with the substrate and the metal is evaporated through the slit to produce the narrow film. Details of this masking procedure are given in Appendix A.

The second method evaluated at this Laboratory involves a micromachining technique. The metal film is evaporated onto a substrate coated with a thin plastic layer in which the desired film geometry has been

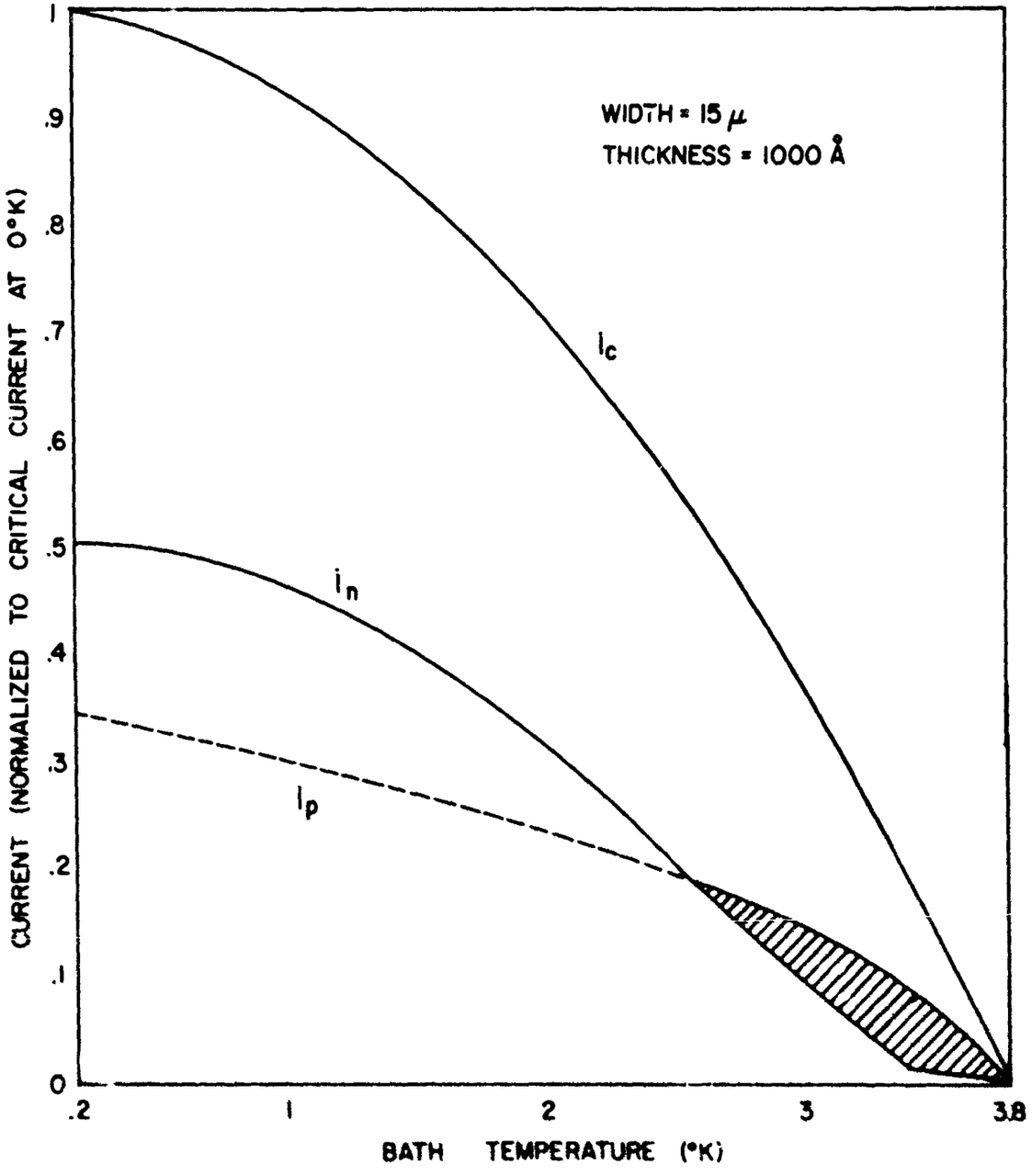

Figure 1.5 First approximation of the threshold curves for a tin film with incident 5 MeV alpha particles; i_c is the critical current; i_p is the threshold for propagating transitions; and i_n is the threshold for formation of a normal region across the film width.

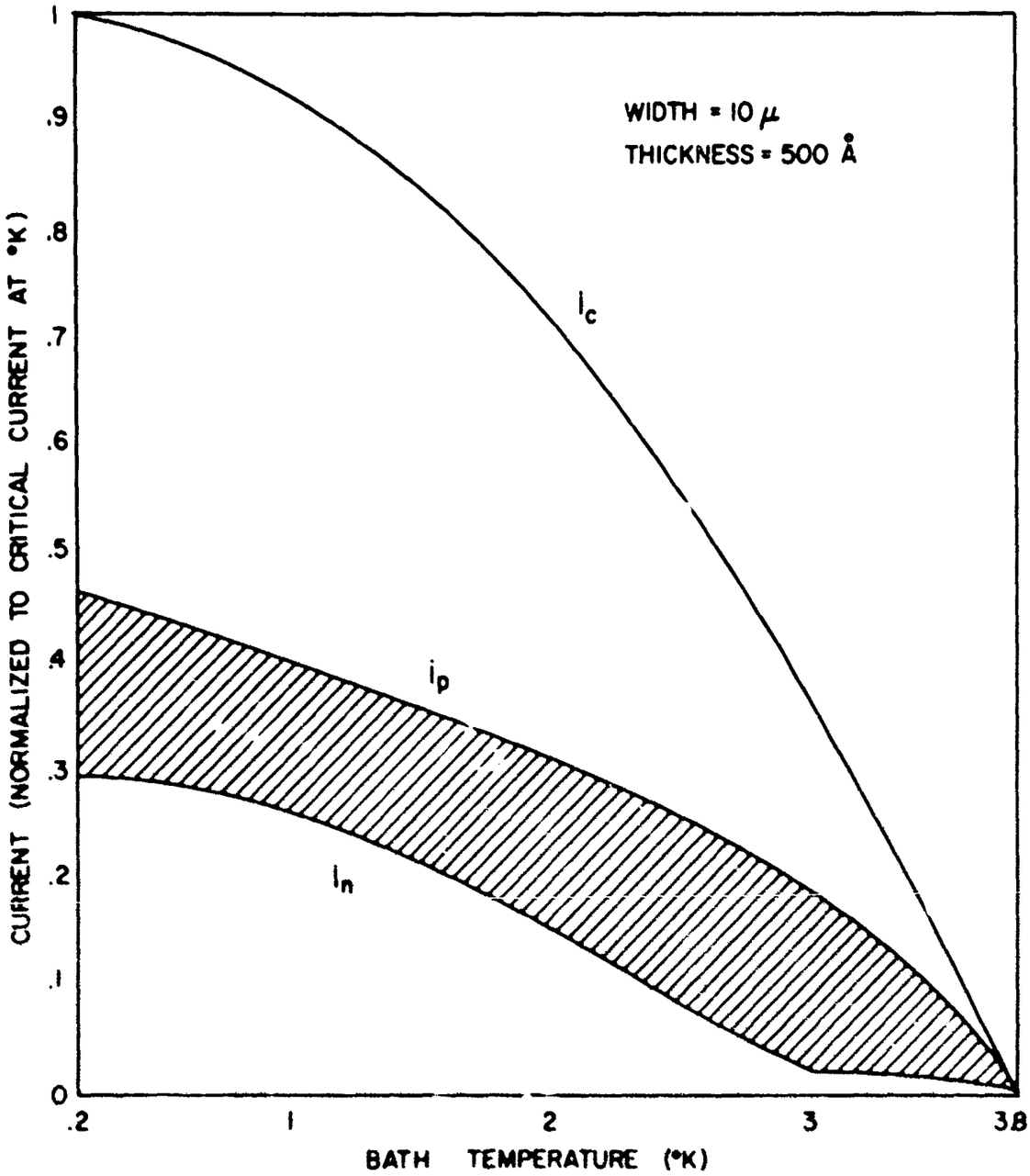

Figure 1.6 First approximation of the threshold curves for a tin film with incident 5 MeV alpha particles; i_c is the critical current; i_p is the threshold for propagating transitions; and i_n is the threshold for formation of a normal region across the film width.

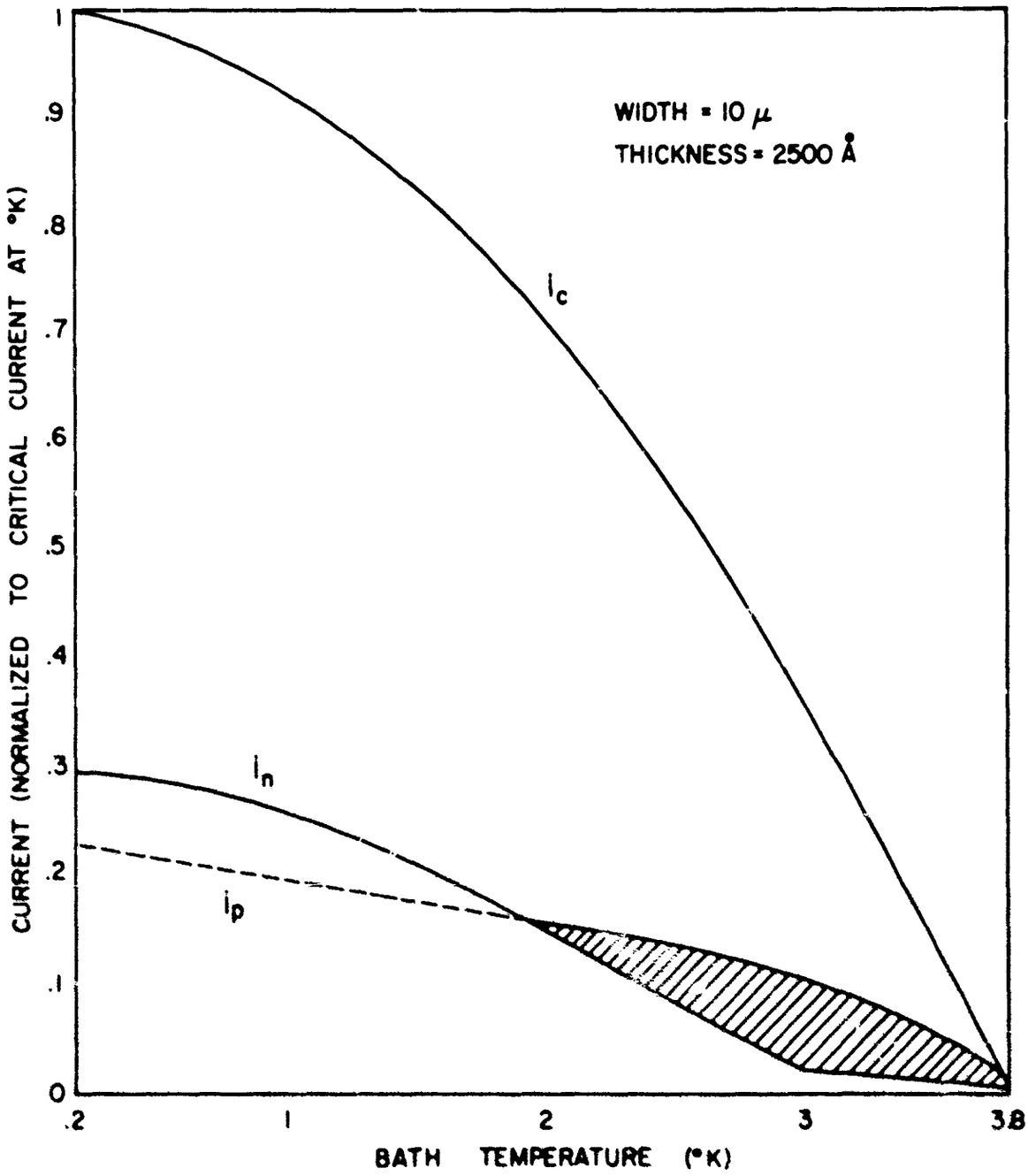

Figure 1.7 First approximation of the threshold curves for a tin film with incident 5 MeV alpha particles; i_c is the critical current; i_p is the threshold for propagating transitions; and i_n is the threshold for formation of a normal region across the film width.

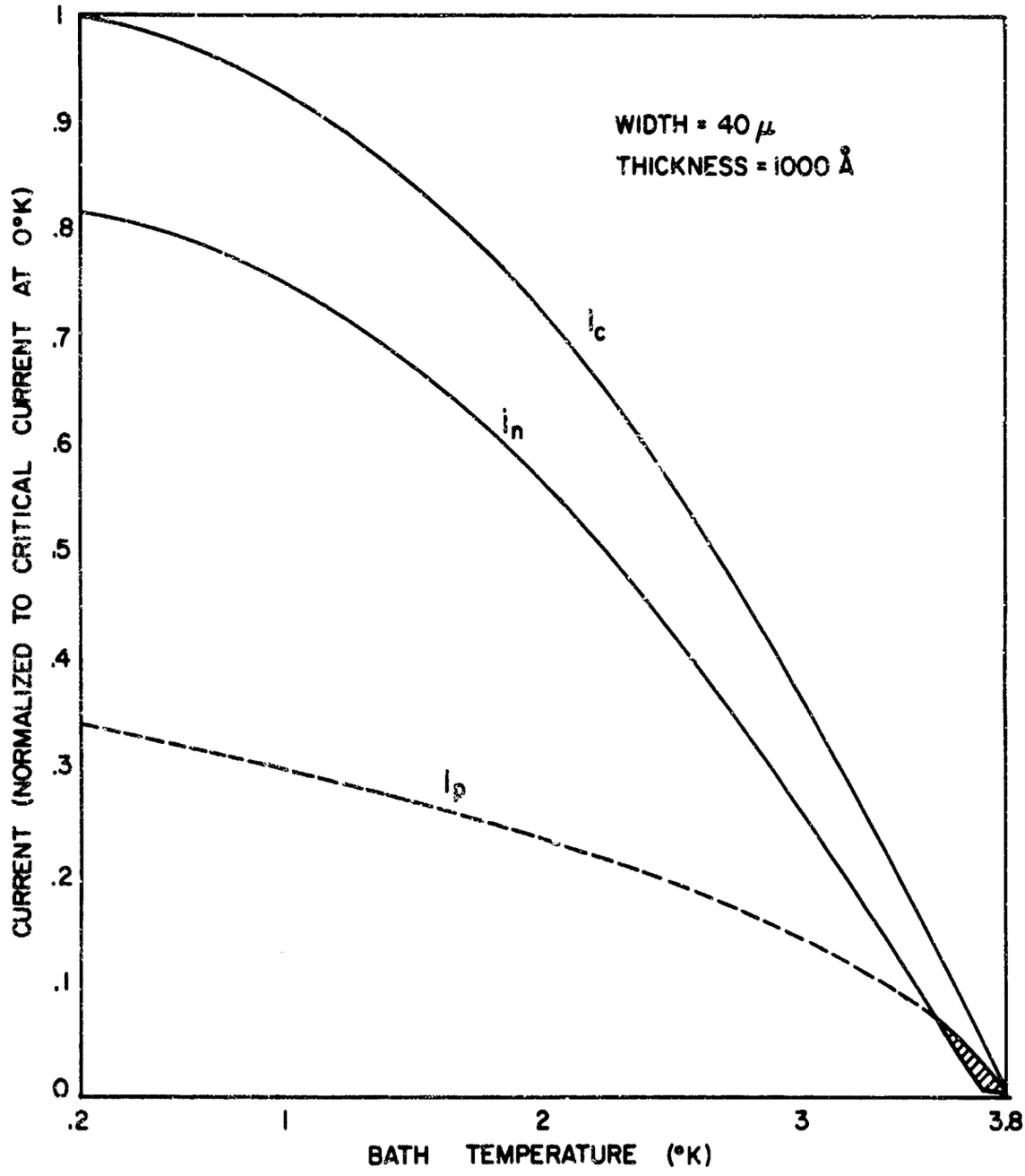

Figure 1.8 First approximation of the threshold curves for a tin film with incident 5 MeV alpha particles; i_c is the critical current; i_p is the threshold for propagating transitions; and i_n is the threshold for formation of a normal region across the film width.

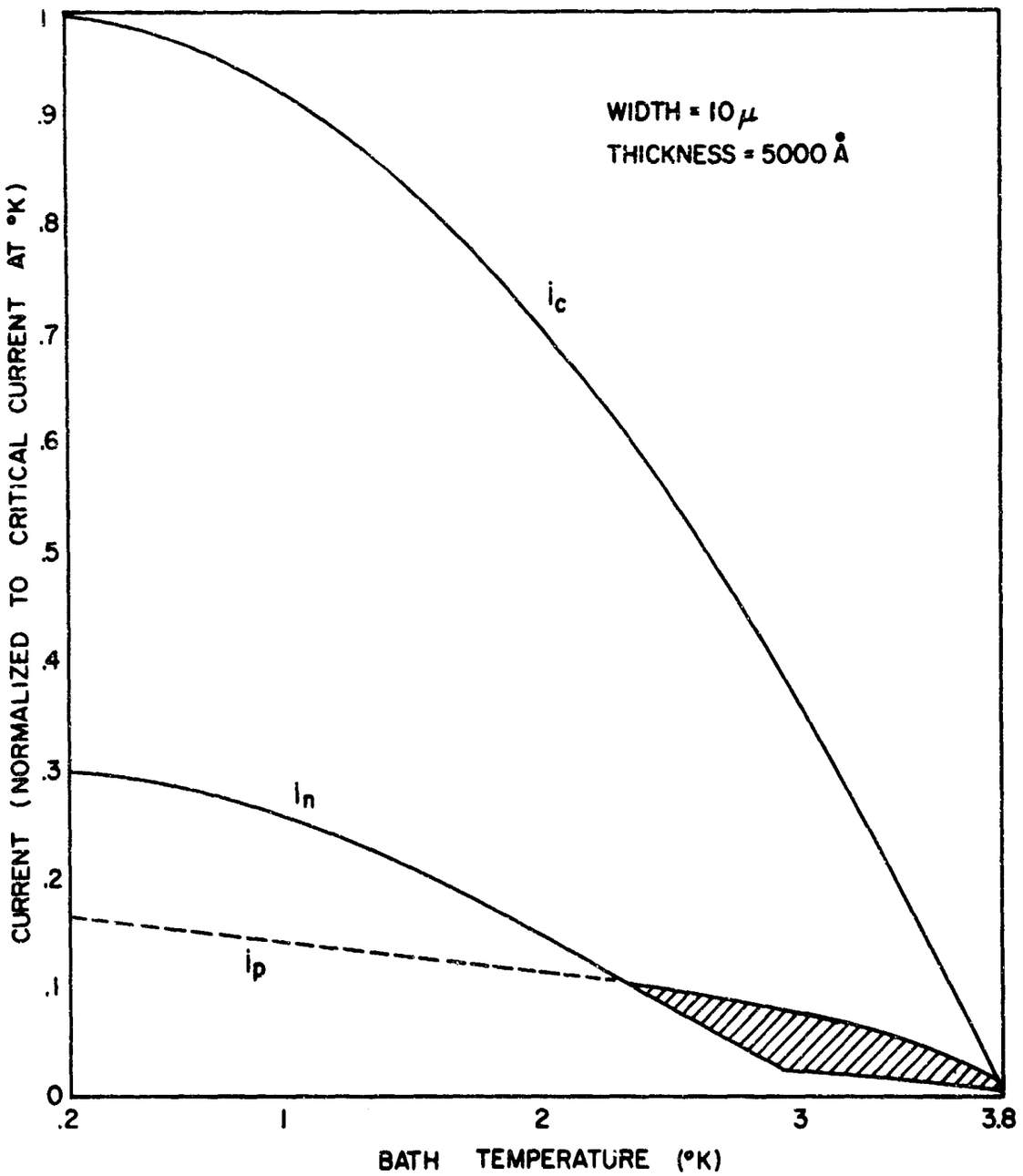

Figure 1.9 First approximation of the threshold curves for a tin film with incident 5 MeV alpha particles; i_c is the critical current; i_p is the threshold for propagating transitions; and i_n is the threshold for formation of a normal region across the film width.

machined. The unwanted portion of the film is then removed by dissolving the plastic coating under it. This is a simple technique that provides reasonably uniform lines, but there is some difficulty in providing a control of film width. This technique is discussed further in Appendix B.

The third approach is in an early phase of evaluation, but holds considerable promise for future work. This approach involves the use of photo-sensitive, chemical-resistant (photo-resist) coatings in a manner similar to that used in fabricating printed circuit boards. The metal film is evaporated over the entire substrate and then coated with a photo-resist layer. An exposure to the proper light pattern and development of the resist leaves a chemically-resistant layer over the area of interest. The remaining film is removed by a chemical etch leaving the desired pattern. Recent work by Government and industry in developing micro-circuitry has established the feasibility of producing such narrow lines by this technique. Lines of 5 μ width and narrower with better than 1/2 μ control of width and uniformity have been attained. Most of the essential equipment for this work has been acquired at this Laboratory and liaison with Army Electronics Command at Fort Monmouth, New Jersey, has been established to aid in process development. Appendix C contains a detailed procedure for photo-resist processing (for thin films) as determined through a visit to the Army Electronics Command.

Prior to evaporation, the substrates were thoroughly cleaned. Several different cleaning techniques were tried and there seemed to be little effect (from different cleaning methods) on the final product as long as the final rinse and drying of the substrate were done carefully. Suitable cleaning was obtained with standard laboratory glassware detergent and a glass-cleaning solution (chromic acid). Alternate cleaning with these two agents coupled with a final rinse in very pure demineralized water and drying under dry nitrogen gas (blown across the surface) produced satisfactory results.

The metal evaporations were carried out in an ion-pumped chamber with initial presure readings between 5×10^{-8} and 10^{-5} torr. (High initial pressures were purposely tried to attain higher resistivities.) A resistively-heated molybdenum boat filled with 0.9999 pure tin was used to accomplish the evaporation onto substrates of single-crystalline quartz (z axis perpendicular to the face of the crystal). The quartz crystals are 1/8 inch thick and 1 inch in diameter with the faces polished to 1/2 wavelength of sodium light. This particular substrate was chosen because the high thermal conductivity permits rapid cooling of the film which is not in direct contact with the liquid helium bath. The source-substrate separation was about 18 cm and the film thickness was monitored with a Westinghouse Quartz-Crystal Microbalance. With this device a somewhat crude control of deposition rate can be obtained and the total thickness of the film can be measured to better than 3 percent accuracy.

The temperature of the substrate was maintained between -5° C and +5° C to prevent the formation of grey tin (an undesirable metallurgical phase of pure tin). The substrate temperature was monitored with a copper-constantin thermocouple. The evaporation rate control and the system pressure can be varied to produce varying film purity. A rapid evaporation at low pressure yields the purest film. This control is rather crude, but a mild spread in film resistivity was obtained. Since the film geometry and dimensions enter into the determination of the resistivity, it is more convenient to characterize the film purity by the ratio of the film resistance at room temperature (300° K) to that at 4.2° K. This ratio is closely related to the residual resistivity of the film which is a measure of the scattering of electrons by impurities. A large resistivity ratio indicates a low residual resistivity (or high purity).

2.2 Temperature Control and Measurement.

The film is cooled through the backing substrate by contact of the substrate with liquid helium. The film under test is mounted on the end of a meter-long stainless-steel (thin-wall) tube which is inserted into the glass liquid-helium dewar from the top. An O-ring flange seals the top of the dewar and the upper section of the dewar is equipped with a port to facilitate control and measurement of the pressure above the helium. A large rotary pump in series with a diaphram-type pressure regulator are used to respectively reduce and control the liquid-helium vapor pressure. Temperature is determined from vapor-pressure tables with a correction being made for the head of helium above the tested film. Two Wallace and Tiernan Vacuum Gauges (complementary ranges) are used to determine the pressure in the dewar to better than 1 mm of mercury. The system is capable of obtaining temperatures between 1.2 and 4.2° K with a stability and accuracy of better than 3 percent. An absolute check of the gauge accuracy was not made, but a check against the lambda point of liquid helium and against the transition temperature of bulk tin indicated better than sufficient precision. In addition, there is a slight overlap in ranges of the two gauges and the two agreed in this region.

2.3 Cryogenic Test Probe.

Figure 2.1 shows a view of the dis working end of the cryogenic test probe. The tin film on the quartz substrate (C) is sealed to the probe end (E) by means of the indium O-ring (D). The threaded brass end (A) and teflon retainer ring (B) are used to hold the substrate and O-ring against the probe end. The coaxial cables used for film measurements are run through the helium bath and pass into the probe at the vacuum feedthrough. Contact to the film is established through spring-loaded contacts in the probe end. A small bit of indium is smeared across the thin-film at the contact points to ensure good contact between the film and the spring-loaded plungers. An alpha-particle source is attached within

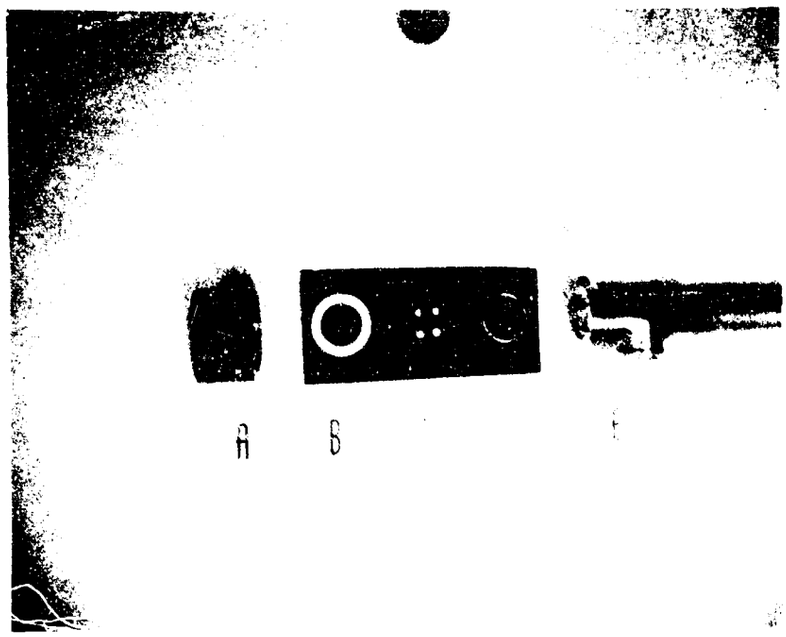

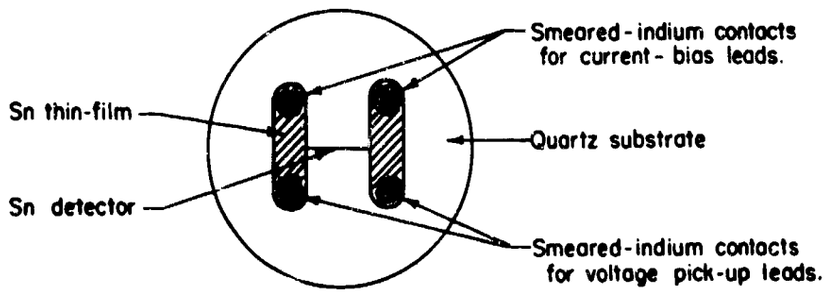

Figure 2.1 Cryogenic Test Probe. The threaded brass end (A) and teflon retainer ring (B) are used to secure the tin film on the quartz substrate (C) with the indium vacuum O-ring (D) against the probe end (E). A pictorial blowup of the film and contacts on the substrate is given below the picture. Contact to the film is by spring-loaded plungers in the probe end.

the probe tube to an externally moveable control rod. The assembled probe is evacuated through a port at the upper end and leak checked prior to each experiment.

The fact that the detector must operate in a vacuum (to avoid attenuation of the alpha radiation in any other medium) creates some difficulty in establishing the film temperature. The quartz backing provides the only cooling of the film and all heat input to the film must be eliminated to permit it to attain the substrate (or helium bath) temperature. Initially the coaxial leads were run down the inside of the evacuated test probe, but this proved unsatisfactory in that these leads acted as heat conductors going directly to the film. By passing the leads through the helium bath, they can be brought to the bath temperature before they reach the film and there is no heat flow to the film. In addition, the temperature of the radiation source must be brought to the bath temperature, because the thermal radiation from it can contribute significantly to heating of the film. A flexible copper-braided strap is used as a thermal connection between the alpha-particle source and the inside of the tube wall, which is at the helium bath temperature. The control rod should be of a material which is a poor conductor of heat since a thermal gradient of 300° K is established along it's length. Thin-wall stainless-steel tubing of 1/8 inch diameter proved to be a satisfactory choice.

The presence of heat leaks can easily be ascertained by operating the probe with a vacuum and without a vacuum (omit the indium O-ring and permit the helium to enter into the test probe) and then determining the transition temperature of a given film in each case. If the two measurements agree, one can be quite sure that all heat leaks have been eliminated or at least reduced to a tolerable level.

2.4 Measurement of Film Characteristics.

The width and length of the film were measured under a microscope with magnifications of x100 to x1000. The width varies along the length of the film and for lack of a suitable means of characterizing the width, the average width is recorded. Films with width variations greater than 20 percent were rejected. The film thickness (see Section 2.1) is obtained from the film thickness monitor after the evaporation.

The film resistance at various temperatures was determined by passing a 100 μA current through the film and measuring the voltage across the film with a Keithley Model 149 Microvoltmeter. The inclusion of contact voltages is avoided by the use of four contacts as indicated at the bottom of Figure 2.1. The input impedance of the voltage measuring

device is high enough to make the contact resistances (in series with the voltmeter) negligible. The resistance of the tin film at 300° K and 4.2° K was recorded. As mentioned in Section 2.1, these resistances were used to form the resistivity ratio, $R_{300}/R_{4.2}$, which is used to characterize the film purity.

The transition from the superconducting to the normal state was monitored with the same resistance measuring arrangement. The transition temperature is taken as the temperature at which the resistance is half its value just above the transition region.

2.5 Measurement of Threshold Curves.

An important aspect of threshold-curve measurements is the problem of observing the transition point without destroying the film. At the currents necessary for testing, the Joule heating of the film in the normal state is sufficient to destroy the film or seriously damage it if the current is not interrupted very quickly after the transition occurs. This is not an important consideration for the observation of recovering pulses, since the entire film does not become resistive. For the purpose of protecting the film, it was necessary to devise a scheme for interrupting the bias current upon sensing a voltage across the film (discrimination against the recovering pulses must be included). Automotive-storage batteries coupled with the circuit of Figure 2.2 were used as a bias supply. Batteries were used in place of a line-operated power supply, because there was concern that the supply ripple might affect the transition to the normal state.

Because the voltage across the film at the transition varies with the bias conditions, it is convenient to use an intermediate triggering circuit. The output of the film between the film and the bias supply is used to trigger an oscilloscope and an output (ramp or square pulse) from the scope is used to trigger the bias supply. The output from the scope is independent of the bias current and thus provides more consistent triggering.

With this triggered supply, the threshold for propagating transitions, I_p, can be readily measured. At a given temperature, the current is gradually increased until a transition is observed. At this point the bias supply is automatically turned off and must be reset prior to subsequent measurements. The relation of the rate of increase of film current and the alpha-source intensity are important in these measurements. If the average period between pulses is large and the rate of increase of the current is high, then it is possible that the current will exceed I_p prior to pulse formation. For low-intensity sources (of the order of 1 μCi) this is a formidable problem and long periods of time are required to make each measurement. Use of a relatively large source at a small separation (100 μCi at 1 cm) facilitates more rapid measurement. Several readings were often taken at a given temperature to ensure that the rate of increase of the current was sufficiently small.

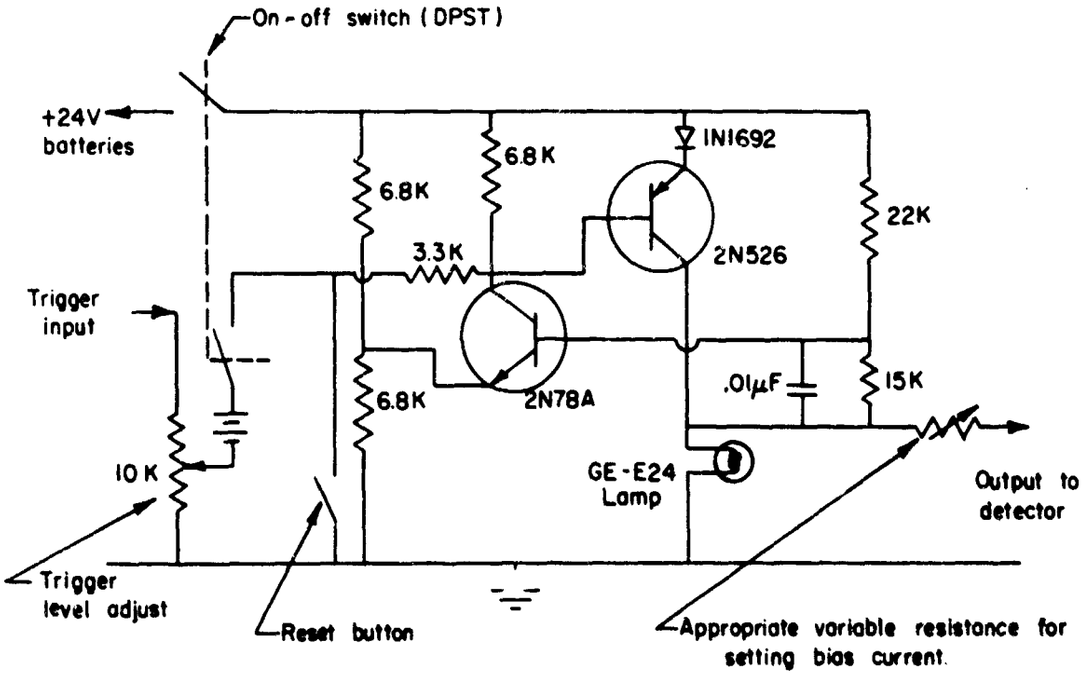

Figure 2.2 Detector current supply. A trigger pulse to the circuit will interrupt the current (until manually reset).

In a similar manner, the d.c. critical current, I_c, is obtained. The alpha-particle source is removed and the di/dt problem is not present. It should be noted that the onset of the normal state with a single current through the detector is not as simple as the transition in the limit of zero current (see Figure 3.1). At currents well below the critical current, a small resistance appears. This resistance appears to be associated with weak points in the film and it is important not to take it as the measure of the critical current. The critical current is that current at which the entire film switches simultaneously to the normal state. At times it is simple to separate the two points, but in the presence of a propagating transition (which can be initiated by the small resistance) this is not quite so simple. All caution has been exercised in trying to obtain a measure of the true characteristic critical current of the film, but such is not ensured, particularly at higher currents. The workers at Atomics International[6] were able to circumvent this difficulty by applying a linearly rising pulse and observing the current at which full resistance was restored. In any event, the results presented here seem to be reasonably close to those obtained by other workers and to the expected theoretical behavior.

The measurement of the threshold for recovering pulses, I_R, as a function of temperature is accomplished by observing the onset of pulse output as the bias current is increased at a fixed temperature. In this respect, the problems encountered are more formidable than might have been expected. The pulses are small (in the 100 μV range) with rather rapid rise times, and the background noise is almost comparable to the pulse height. The necessity of bringing the cable through the probe wall in the liquid-helium bath, along with the problem of coupling to the detector of plane geometry, results in a substantial open loop which introduces electromagnetic noise into the circuit. That this is the origin of the noise was checked by comparing this noise against that picked up in a small open loop (of comparable area) at the end of a coaxial cable. By redesigning the testing probe (coaxial feed-through) and incorporating the detector into a coaxial line, this noise could certainly be reduced to a more tolerable level.

The bias current is introduced via a coaxial cable since the pulse will see the current leads as an exit path. Both cables are terminated at their other end with the characteristic impedance of the cable (50 ohms in this case). It is esential to terminate the current-supply cable properly to avoid reflections of the pulse.

The pulse is amplified prior to viewing by a Keithley Model 107 Pulse Amplifier that has a voltage gain of 10, 100, or 1000. The pulse is then viewed (with further internal amplification) with a Tektronix Model 585 Oscilloscope. The limiting rise time of the combined circuit is somewhere between 4 and 5 ns.

3. RESULTS AND DISCUSSION

3.1 Film Characteristics.

The physical characteristics of the three films for which data will be presented are given in Table 3.1. The control of resistivity (or resistivity ratio) by evaporation time and pressure can be seen. The value of 19.4 for the resistance ratio of film No. 35 is associated with the fastest evaporation at the lowest average pressure (the average pressure is presented, since the pressure increases during the evaporation). Film No. 40, with a resistance ratio of 14.2, has the longest evaporation time of the three and the highest average pressure.

TABLE 3.1 PHYSICAL CHARACTERISTICS OF FILM

Film No.	Width	Thickness	Length	Res 300° K	Res 4.2° K	$\frac{R_{300}}{R_{4.2}}$	Resistivity 4.2° K	Avg Pres	Evap Time	Trans Temp
	μ	Å	cm	Ω	Ω		μΩ-cm	torr	s	°K
35	30	1090	0.42	300	15.5	19.4	1.10	7×10^{-7}	20	3.83
38	18	1180	0.47	570	30	19	1.15	7×10^{-7}	30	3.85
40	14	1190	0.47	655	46	14.2	1.37	5×10^{-6}	60	3.81

The variation of the transition temperature from sample to sample is attributed to the combined effects of impurities and stress in the film due to unequal contraction of the film and substrate. Values of T_c between 3.78 and 3.85° K were recorded and should be compared with the bulk value of 3.72° K. The transition of the film to the superconducting state is somewhat broader than that for pure bulk tin. This can be attributed to the film stress and impurity and to the effect of the passage of the measuring current. The variation of resistance with temperature just above the transition is undetectable; thus, the neglect of such dependence is justified.

The range of resistivities is fairly narrow, going from 0.85 to about 1.40 μ ohm cm. There appears to be no dramatic dependence of the operational characteristics on the film resistivity for this small range. If the

film characteristics are dominant in arriving at the size of the normal core, then there would be some noticeable effect of film resistivity on detector operation. The effective width of the film, from the standpoint of the threshold measurements, is probably somewhat smaller than the average value of the width. This is because the threshold is undoubtedly that for the narrower regions of the film.

3.2 Detector Thresholds.

The detector threshold curves for the three different widths of Table 3.1 are seen in Figures 3.1, 3.2, and 3.3. The curves in Figure 3.1 are cut off at 2.7° K because the sample was damaged by failure of a component of the protection circuit. The progressive decrease of the recovering-pulse region with increasing width is readily seen in the three figures. The two wider films are in reasonable qualitative agreement with the predictions of Section 1.3, but the 14-μ-wide film of Figure 3.1 has extra bends in the two lower curves for which there is no ready explanation. There seems to be little question that the enclosure of the recovering-pulse region is associated with the crossing of the two types of threshold curves. The width at which crossing begins to occur is, of course, set by the value of the thermal conductance of the boundary, κ, which is adjusted to give reasonable agreement between theory and experiment for narrow films. The value of κ obtained in this manner (3 W cm^{-2} deg^{-1}) is quite reasonable, but it would be interesting to make an independent measurement of this quantity to check the validity of the procedure. The fact that the enclosed nonpropagating-pulse region becomes vanishingly small as the film width exceeds 50 μ is in qualitative agreement with the theory.

At lower temperatures, the threshold of the wider films (see Figures 3.2 and 3.3) levels off more rapidly than the theory predicts. The theoretically predicted threshold is that for formation of a normal region across the film width. In this region, this threshold curve is above the threshold for propagation. Any other disturbance that causes the formation of a resistive region will cause propagation and give a false reading. For the wider films, it seems likely that the high self field at the film edges will cause flux to flow into the film and thus produce resistance in the film. This problem of flux flow in superconductors (or flux jumps) is of considerable importance and treatments of it can be found throughout the literature.[9,10] The point is that (for wider films) the threshold below the temperature of the crossing point may reflect some propagational initiation by means other than alpha-particle passage.

Note that not all of the threshold curves exhibit the smooth behavior indicated by the data presented. At times irregular bumps appear in the threshold curves, particularly in the vicinity of the helium lambda point. This would seem to indicate that the change in the boundary (between the substrate and the liquid helium) flow of heat affects the behavior of the detector. This is somewhat disturbing, since simple calculations of the

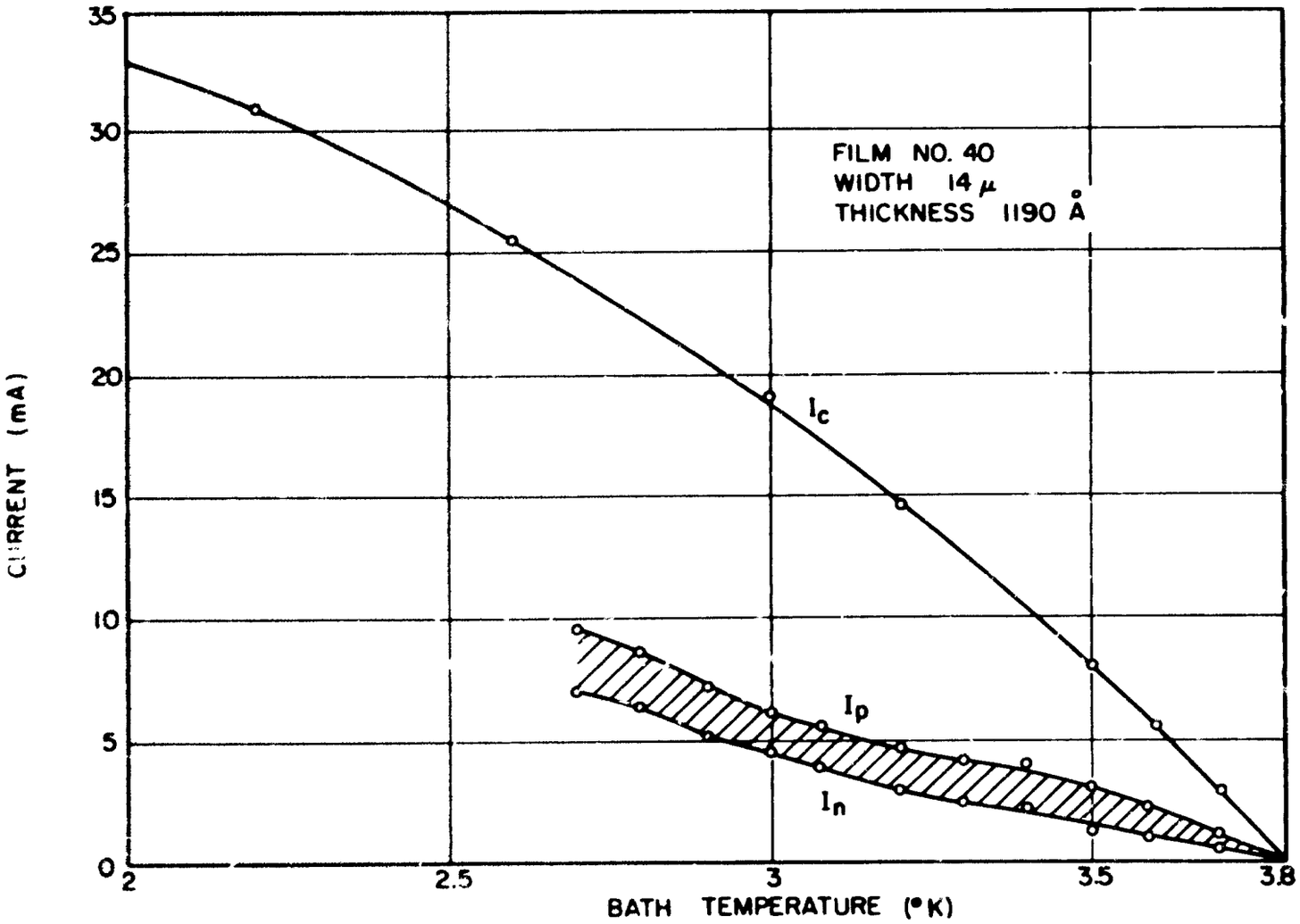

Figure 3.1 Experimental detector threshold curves. I_c is the dc critical current, I_p is the threshold for propagating pulses, and I_n is the threshold for self-recovering pulses. The shaded region is that region in which recovering pulses occur.

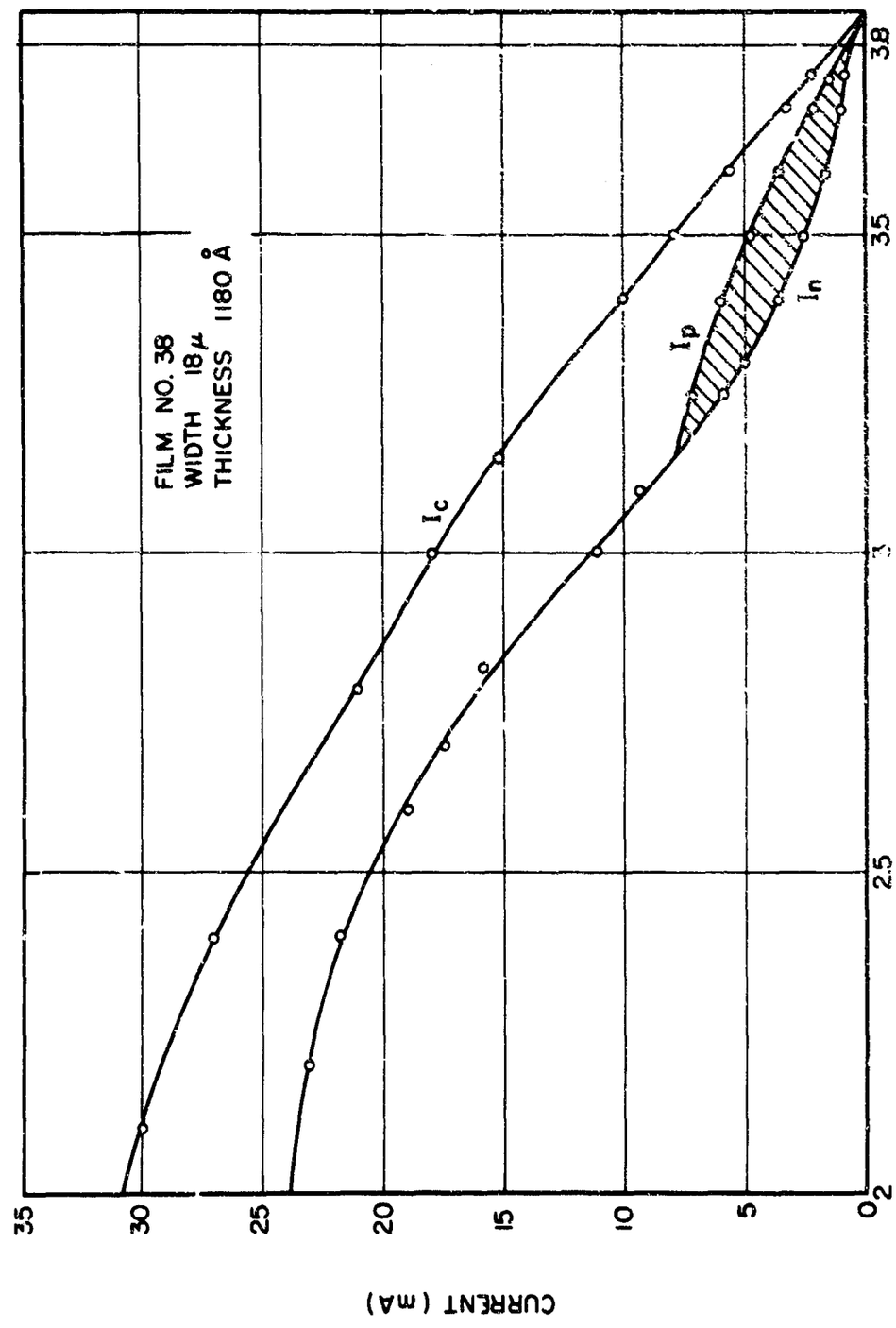

Figure 3.2 Experimental detector threshold curves. I_c is the dc critical current, I_p is the threshold for propagating pulses, and I_n is the threshold for self-recovering pulses. The shaded region is that region in which recovering pulses are observed.

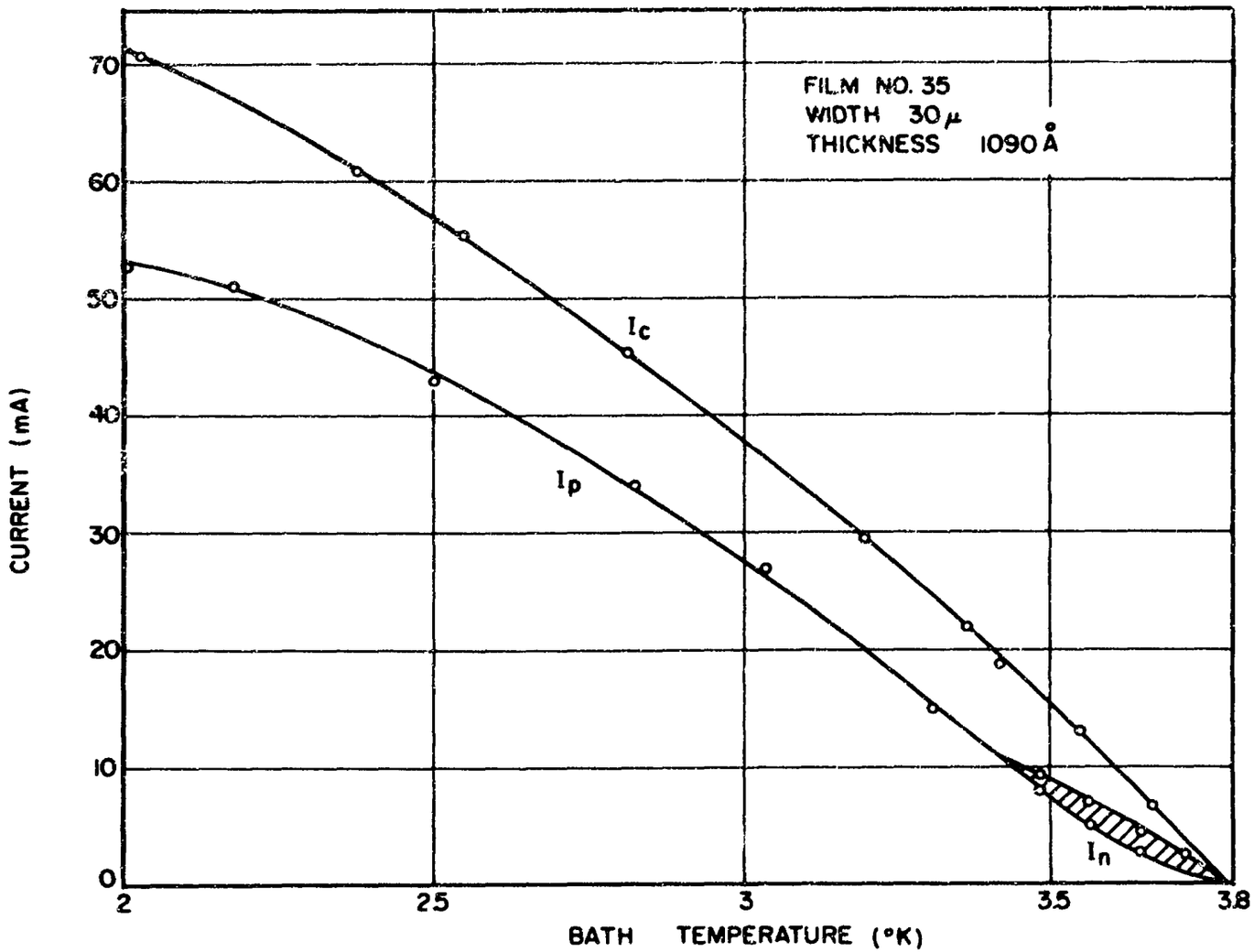

Figure 3.3 Experimental detector threshold curves. I_c is the dc critical current, I_p is the threshold for propagating pulses, and I_n is the threshold for self-recovering pulses. The shaded region is that region in which recovering pulses are observed.

heat flow through the substrate indicate that the liquid helium-quartz substrate interface should have no such effects on the threshold curves. Perhaps this behavior is associated with some undetected heat leak that is altered at the lambda point.

At first glance, it would seem logical to present the comparison of the values of r_c obtained from theory and experiment (see Section 1.2.3). This presentation has been avoided because the experiment presented in the next section is damaging to the foundations of the theory. However, for the sake of argument, such a comparison is given in Figure 3.4. The surprising agreement should in no way be taken as a confirmation of the theory. In fact, this agreement should be considered extremely fortuitous. Of course, the same theory has been used to calculate the threshold for pulse formation, I_n, but the intent of these calculations is simply to systematize the detector behavior. The general qualitative features of the thermal slump, with the accompanying increase of r_c with increasing bath temperature, are expected to remain intact even if the theory cannot be considered to be quantitatively accurate. Thus, the use of the theory to generate a qualitative understanding of the detector thresholds is not unwarranted.

3.3 The Split-Film Experiment.

Recently, the group at Atomics International[11] has performed an experiment that sheds light on the basic assumptions of the operational theory. They operated two independent detectors in close proximity and found an unexpected coupling through the substrate. Their sample was constructed by laying a thin-quartz fiber down the center of the razor-blade mask, thus producing two narrow films separated by the width of the fiber. Each film was biased independently with separate monitoring for self-recovering pulses. The films were each about 9 μ wide and the separation was 6 μ. According to the theory, these two films should operate completely independently with very low coincident-pulse rate for modest source intensity. However, a very large fraction of the pulses were observed in coincidence, indicating that the film and substrate are intimately coupled. Apparently the heated core spreads in the substrate and creates a normal region in the second film as well as the one upon which the particle is first incident. A slight time separation between pulses (in coincidence) is observed and this may be tied to the velocity of the heat flow in the substrate. Thus, the basic assumption in the theory of the independence of film and substrate is found to be invalid. The experiment which negates this assumption would seem to be a useful tool in studying the dynamic behavior of the heated region in the substrate.

The strong dependence of detector behavior on the material used as a substrate is another result which is damaging to the assumptions of the theory. Pulses from films backed by fused glass substrates are much

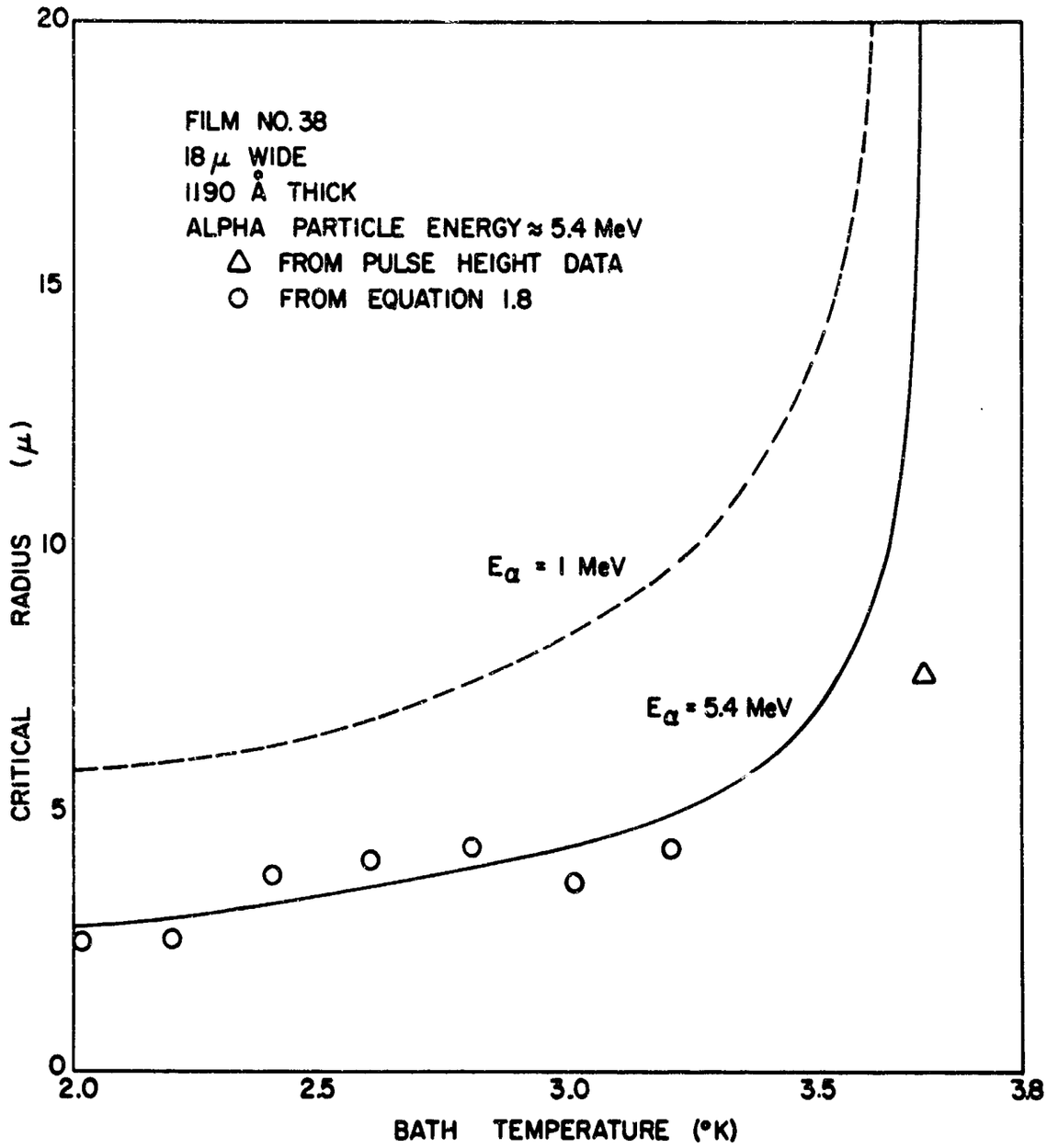

Figure 3.4 Comparison of experimental values of r_c with theory. Because of problems with the foundation of the theory, this fit must be considered fortuitous. For comparison, the results expected for 1 MeV alpha-particles are presented.

broader and slow rising and the threshold curves are such as to produce much smaller recovering-pulse regions. The fact that the pulses resulting from irradiation with monoenergetic alpha-particles are not uniform in amplitude may well be associated with this coupling of the film and substrate. It would seem that a particle hitting off the film could produce a pulse which is somewhat smaller than one hitting the direct center of the film. Thus, a spread in pulse heights could result from single energy events.

The coupling between film and substrate must be a lattice coupling (acoustic mismatch at the boundary) and thus the electrons and lattice must readily share their energy. Hence, the assumption that only the electronic components of the thermal conductivity and the specific heat enter the calculation is also invalid. It may be that the growth of the heated region in the substrate is the dominant factor in the detector and that the apparent agreement between the experiment and the ungrounded theory is related to a coincidental growth of the thermal distribution in the quartz.

4. CONCLUSIONS

This work has shown the feasibility of the concept of particle detection by means of local thermal transitions in superconductors. The simpler parameters governing the detector's operation have been studied and the speed and position sensitivity of the detector have been established. There is, as yet, no successful theory which fully accounts for the observed behavior, but experiments do lend significant support to most of the qualitative features of the thermal slump model. In particular, the threshold curves for the detector are quite consistent with those calculated in Section 1.3.

The importance of the substrate is apparent from the split-film experiment. Further evaluation of the detector must rest on the development of an adequate quantitative description of the coupled growth of the heated regions in the film and substrate.

The attempt to systematize the detector behavior has resulted in the threshold-curve equations given in Section 1.3. The dependence of the thresholds on the width, thickness, resistivity, boundary thermal conductance, and several other parameters can be extracted from these equations. Thus it is now possible to consider adjusting these parameters by appropriate selection of material, impurity content, width, and thickness, to obtain the best possible arrangement for a particular application.

5. SUGGESTIONS FOR FUTURE WORK

The research on this detector has opened up many possible approaches to further development of the concept. Of prime importance in any future endeavors is the establishment of the film-substrate relation in the dynamics of the thermal slump. The type of coupling, means of characterizing the energy transport in the substrate, the development of the slump in the film, and the composite relation of all these items must be established to complete the description of the detector.

The split-film experiments seem to offer a number of possibilities in this regard, not the least of which is the actual mapping of the growth of the heated region in the substrate. The time between pulses (from the same event) along with the ratio of the pulse heights should provide such information. These types of experiments, along with very careful comparisons of detector behavior on different substrates, should elucidate, experimentally, the dynamics of the thermal slump.

In developing the theory, some profit might be reaped from assumptions at the opposite extreme of the question of film or substrate dominance. One could assume that the substrate is completely dominant and that the film temperature is identical to that at the surface of the substrate. For the quartz single crystals this will have to lead to an approach other than classical thermodynamics,[12] since the phonon mean free path in this material is large compared to the dimensions characterizing the thermal slump. In glass such calculations might be applied in a classical manner.

The question of film or substrate dominance is yet unsettled and it may be that neither really dominates and that the dynamic coupling of the two must be considered. Some hint as to the magnitude of the coupling might be obtained from the estimate of the thermal conductance of the boundary obtained in Section 1.3.

In actually building a useable detector, it would appear that innovation is the key word. As an example, the energy dependence of the detector might be realized if the film lies on a ridge of its own width, thus eliminating those events that do not actually penetrate the film. Even if the film is not dominant in the theory, the pulse height should be related to the stopping power in the substrate or some suitable combination of the stopping power of both. A tighter coupling of the film to the bath (increased κ) will surely expand the region of recovering pulses, since the threshold for propagation will occur at a higher current. This might be accomplished by evaporating the film onto an oxide-coated metal substrate (which may be a superconductor and thus simultaneously provide a ground plane). The detector area can be increased by increasing the length of the detector and a number of possible approaches exist here.

The thermal spike occurring in the superconductor may be detectable by means other than observing the voltage drop across the normal region. A small area tunneling junction (superconductors) biased in a region of low transmission (voltage less than the energy gap voltage) should offer a reasonable detection scheme. The thermally excited electrons would cause an increase in the tunneling current over the normal core region. The current through the junction should be proportional to the integrated tunneling current over the thermal profile in the junction. This scheme offers the advantage of being void of the Joule heating normally important after the pulse is formed. Thus, the entire pulse shape as a function of time should be a measure of the dynamic behavior of the thermal spike. While the Joule heating in the line-type detector is useful in providing position sensitivity (propagating transitions), the problem of attaching significance to the pulse shape is obscured by it.

Another approach might use the Meissner Effect of Type I superconductors, that is, the exclusion of magnetic field by the superconducting phase of the metal. The flux excluded from the superconductor below the transition temperature would collapse into the superconductor (in very small regions) upon incidence of an ionizing particle. Any means of detecting the flux change, or the rate of movement of flux would essentially detect the particle. The example of the preceding paragraph should definitely be feasible, while this latter is offered only as an example of a different approach to the problem.

A definite need exists to make some practical improvements in the existing fabrication techniques and testing procedures. The problem of uniformity of film width and adequate control and reproducibility of all film parameters should be overcome. In this respect, perhaps the photo-resist approach to film fabrication will be found best. Certainly the production of detectors of more exotic geometry will not be accomplished by simple masking techniques. Crittenden[12] has pointed out, however, that the improvement of the edges of the detector (better uniformity) may not solve all the problems, since unresolvable scratches (from polishing) in the substrate surface will probably result in weak spots along the film. Scratches of depth comparable to the film thickness with sufficiently steep walls will produce non-uniform film thickness that should cause the film to behave as if there is a nick in the width of the film. Hence, the desire for better samples should be tempered with the realistic expectations of massive efforts in this direction.

A more pressing immediate need is that of reducing the noise level of the detector. As pointed out in the text of the report, the origin of this noise is believed to be just that coupling by means of an open loop to electromagnetic noise in the room. Incorporation of the detector in some sort of coaxial line to eliminate the open loop should be of considerable help.

APPENDIX A

STRAIGHT-EDGE MASKING

This appendix contains a detailed description of the fabrication and use of straight-edge razor-blade masks used in preparation of the narrow thin-film detectors.

Thin Gillette blades were chosen for the masks because their smaller thickness should result in reduced penumbra at the line edges. The edge of this blade is not necessarily better than others considered. The blades are broken (this seems to be better than trying to cut them) into short pieces of about 1/2 cm length. The blades are secured with Duco cement to a lucite disk with a cutout similar to that shown at the bottom of Figure 2.1. The cutout portion is used to define the contact areas. The first blade is secured and the glue is permitted to dry. The second is then placed in position with a small dab of glue under it. This blade is then maneuvered, under a microscope, into a position parallel to the first blade with the proper separation. The glue is then permitted to dry. The placement of glue prior to positioning is dictated by the difficulty of gluing the blade down after positioning it (without disturbing its position).

At this point there usually seem to be at least several projections of foreign materials into the gap. Such protrusions are not tolerable since they produce significant indentations into the evaporated film. If the material is loose, it can be blown or rinsed (with acetone or alcohol) from the mask. A particularly effective means of removing these projections is accomplished through an electro-erosion technique.[13] The use of this technique dictated the choice of an insulator as the mount for the blades. A 60-cycle alternating voltage is applied across the gap and the narrower portions experience breakdown and erosion due to the higher electric field. Loose particles seem to be polarized and swept away by the alternating field. The voltage is increased to several hundred volts where the breakdown just becomes visible under a microscope. A series resistance of 10 MΩ prevents excessive current flow and thus keeps the erosion rate at a reasonable level. Several minutes under this treatment will not only remove all loose particles from the gap, but will erode away any metallic projections into the gap. The technique is quite effective in removing sharp bumps in the blade edges, but will not effectively handle very gentle variations in the width of the gap. The sharp points at the end of each blade are rounded off.

Spiel, et al.[5] have found that the initial straightness of the blade edge can be improved significantly by stroking the blade against an acetone-wetted piece of microscope glass. The blade is held perpendicular to the glass and the blade is slid along the glass as if trying to slice the glass with the full length of the blade.

It is important that the mask is in good contact with the substrate during the evaporation and a reasonably large substrate-source separation is desirable. This masking technique is extremely tedious and requires considerable patience and practice on the part of the experimenter.

APPENDIX I

MICROMACHINED MASKS

This appendix describes the evaluation of a technique suggested in the literature[14] which has certain limited possibilities. The evaluation is reasonably complete, but the technique can certainly be pushed beyond the limits encountered.

The coating of the film prior to the evaporation is with a very thin film of Carbolin K-83 Paint. The paint is thinned with 10 parts of acetone and applied by dipping the substrate or pouring the paint over the tilted substrate. The plastic coating is permitted to air dry for at least 8 hours. Shorter drying periods resulted in unsatisfactory behavior of the film during the machining.

The wide contact areas can be easily scratched into the coated substrate with a small knife. Reasonably good straight lines were scratched in the plastic coating using a straight edge and a new razor blade. With the plane of the blade perpendicular to the substrate and the blade edge making a small angle with the substrate surface, the blade is drawn along the straight edge producing a narrow slit in the plastic film. A small pointed tool driven by a screw could possibly be used for this same purpose.

The metal film is then evaporated over the entire mask and the substrate is then soaked in acetone for 5 to 10 minutes to dissolve the plastic. The film over the dissolved plastic is gently rinsed away leaving the desired narrow line. While surprisingly good lines as narrow as 5 μ were produced, it was difficult to control this width. This is by far the quickest and simplest approach to the fabrication of these detectors.

APPENDIX C

PHOTO-RESIST TECHNIQUE

This appendix describes a detailed procedure for a photo-resist process which should form a basis for establishing this type of program at the Laboratory. The nature of micro-geometry work with photo-resist is such as to classify it as an art rather than an everyday tool. The approaches to its application are as numerous as the labs employing it. Thus, the program outlined here will necessarily incorporate those peculiarities of the process of the Army Electronics Command.

The chemicals used are produced by Kodak and are: Kodak Thin-Film Resist (KTFR), Kodak KMER Developer, and Kodak KMER Thinner. J-100 Resist Strip from Litho Aluminum Products Company is a suitable stripper for the developed photo-resist. All chemicals are filtered using Millipore filters to 0.8 μ except the KTFR which is filtered in steps to 1.5 μ. The viscosity of the KTFR is such as to require a Pressure Filter Apparatus to accomplish the filtering. The majority of the solids can be removed from the KTFR prior to filtering by centrifuging it for about an hour at 2000 rpm.

A suitable light source for the exposures is a Sylvania Sun Gun II Movie Light which incorporates a halogen filled bulb. The resist is sensitive in the near ultra-violet region. A clean bench is a necessity and temperature and humidity control are extremely desirable. Sprayers for application of the developer and rinse solution are desirable but not essential. The KTFR is most conveniently applied by spinning the substrate. A very good high acceleration spinner is manufactured by Headway Research Incorporated.

All gas for blowing off the chemicals and pressurizing the sprayers and filtering apparatus is passed through 0.8 μ filters. A hot plate adjustable to 140°C is necessary for baking steps in the procedure. The KTFR prior to developing should be handled only under darkroom safelights. The step by step procedure follows.

A. Substrate Cleaning. Good results depend critically on the adhesion of the resist to the substrate. To this end, all efforts must be made to assure that the substrate (before coating) is clean.

1. Apply resist immediately after evaporation of the metal film.

2. The substrate should be vacuum baked at about 150° F for one half hour if it has been out in air for more than a few hours.

B. Photo-resist Coating.

1. For best results use an eyedropper to cover the substrate with resist and use a rapid acceleration to bring the substrate to 6000 rpm for about 20 seconds. The KTFR dilution (see note at end) and the spinning time determine the resist thickness, so this spinning time will vary with requirements.

2. Spin coating at slower speed will work, but not as well as the above method. Poor acceleration will require that the resist be applied to the already spinning substrate, a somewhat questionable approach.

C. Drying and Prebaking.

1. Dry the coated substrate for at least one half hour at room temperature. Then bake on a hot plate for 15 to 25 minutes at 120° F.

2. Heat should always be applied from the bottom to assure that a dry layer does not form on the top and prohibit the exit of the solvents below.

3. Let the substrate cool to room temperature before exposure.

D. Exposure.

1. The mask (photographic negative of the desired pattern) should be in direct contact with the substrate to produce a contact print.

2. Exposure depends on resist thickness, light intensity, and desired definition. For a 2 μ thick film of KTFR, an exposure of 15 seconds at about 8 inches with the Sylvania Sun Gun will provide a fairly good image.

3. The resist is not damaged by overexposure. But excessive exposure results in diffused edges and some transmission and exposure in undesired areas.

E. Development and Rinse.

1. Develop for 30 seconds in a spray of KMER developer. Then rinse using an eyedropper in deionized water.

2. Rinse for 15 seconds with a mixture of 1 part isopropyl alcohol and 4 parts KMER developer.

3. Rinse in deionized water again and blow dry (gently) with filtered nitrogen gas.

4. Resist layers thicker than a few microns will require correspondingly longer develop and rinse times.

5. If spray equipment is not available, a dip development technique may be suitable. Application of chemicals with an eyedropper is recommended. A flushing action should be utilized to carry away the developed resist. Harsh agitation of the substrate in a bath may wash away the desired image.

F. Post-bake.

1. Bake on hot plate for 20 minutes after drying.

2. Cool to room temperature prior to etching away the undesired film.

G. Etch.

The etching of Sn can be accomplished with a solution of Ferric Chloride. The solution strength should be varied to obtain a slow etch (1- or 2-minute).

NOTES: The viscosity of the KTFR and the spinning time determine the thickness of the resist. Information concerning the thickness relation to dilution and viscosity can be obtained from a Kodak publication.[15] The KTFR should be diluted with the KMER Thinner prior to the filtering of the KTFR.

For a 1- or 2-μ thick film of resist, a dilution of 7 parts (by volume) of KTFR to 3 parts thinner and a spinning time of 20 seconds at 6000 rpm is suitable. This thickness of resist seems to be adequate for images in the 10- to 30-μ range.

The process above is based on Kodak chemicals. A process using Azoplate chemicals (distributed by Shipley Company Incorporated) may also be of significant interest. The Azoplate resist is more difficult to coat on the substrate, but there is some evidence that better definition can be obtained with it.

REFERENCES

1. D. H. Andrews, R. D. Fowler, and M. C. Williams, Phys. Rev. 76, 154 (1949).

2. N. K. Sherman, Can. J. Phys. 40, 372 (1962).

3. N. K. Sherman, Phys. Rev. Letters 8, 438 (1962).

4. D. E. Spiel, R. W. Boom, and E. C. Crittenden, Jr., Appl. Phys. Letters 7, 292 (1965).

5. D. E. Spiel and R. W. Boom, Superconducting Nuclear Particle Detector, Atomics International Report, AI-65-36 (1965).

6. J. B. Greer, D. B. Sullivan, and W. R. Van Antwerp, Superconducting Thin-Film Nuclear-Particle Detectors, 5th Army Science Conference Proceedings 375, (1966) AD 634 615.

7. W. H. Cherry and J. I. Gittleman, Solid State Elec, 1, 287 (1960).

8. R. F. Broom and E. H. Rhoderick, Brit. J. of Appl. Phys. 11, 292 (1960).

9. A. R. Strand, C. F. Hempstead, and Y. B. Kim, Phys. Rev. Letters 13, 794 (1964).

10. J. Bardeen, Phys. Rev. Letters 13, 747 (1964).

11. D. E. Spiel, R. W. Boom, and E. C. Crittenden, Jr.; Superconducting Nuclear Particle Detector; NDL-TR-87 (AI-67-74), August 1967; US Army Nuclear Defense Laboratory, Edgewood Arsenal, Maryland; Unclassified.

12. E. C. Crittenden, Jr. (private communication).

13. F. J. Bontoft, J. Sci. Instrum. 42, 825 (1965).

14. T. K. Hunt, Phys. Rev. 151, 325 (1966).

15. Kodak Seminar on Microminiaturization, Eastman Kodak Company, June 3 and 4 (1965).

UNCLASSIFIED

Security Classification

DOCUMENT CONTROL DATA - R & D

(Security classification of title, body of abstract and indexing annotation must be entered when the overall report is classified)

1. ORIGINATING ACTIVITY *(Corporate author)*

US Army Nuclear Defense Laboratory
Edgewood Arsenal, Maryland 21010

2a. REPORT SECURITY CLASSIFICATION

UNCLASSIFIED

2b. GROUP

3. REPORT TITLE

A SUPERCONDUCTING THIN-FILM NUCLEAR-PARTICLE DETECTOR

4. DESCRIPTIVE NOTES *(Type of report and inclusive dates)*

5. AUTHOR(S) *(First name, middle initial, last name)*

Donald B. Sullivan

6. REPORT DATE	7a. TOTAL NO. OF PAGES	7b. NO. OF REFS
October 1967	58	15

8a. CONTRACT OR GRANT NO.	9a. ORIGINATOR'S REPORT NUMBER(S)
b. PROJECT NO. 1L013001A91A	NDL-TR-93
c.	9b. OTHER REPORT NO(S) *(Any other numbers that may be assigned this report)*
d.	

10. DISTRIBUTION STATEMENT

This document has been approved for public release and sale; its distribution is unlimited.

11. SUPPLEMENTARY NOTES	12. SPONSORING MILITARY ACTIVITY
	Department of the Army

13. ABSTRACT

Recent advances in theory and development of a superconducting nuclear-particle detection technique are presented. A review of previous theory as well as recent theoretical work is included. Experimental results obtained at US Army Nuclear Defense Laboratory and through contract with Atomics International, a division of North American Aviation, are compared with the existing theory. The report is intended, not only to present results of recent work, but also to provide a summary of all developmental work. The problems encountered in the research are discussed and some suggestions are offered as possible paths to solutions.

DD FORM 1 NOV 68 1473 REPLACES DD FORM 1473, 1 JAN 64, WHICH IS OBSOLETE FOR ARMY USE.

UNCLASSIFIED

Security Classification

14. KEY WORDS	LINK A		LINK B		LINK C	
	ROLE	WT	ROLE	WT	ROLE	WT
Detector, nuclear particle						
Nuclear particle detector						
Superconductors						
Cryogenics						